Ocean Engineering 356 (2026) 125210

Contents lists available at ScienceDirect

Ocean Engineering

journal homepage: www.elsevier.com/locate/oceaneng

Research paper

Integrated performance and risk assessment of co-located wave energy and offshore aquaculture systems under operational uncertainty

Minghan Bao [a], Ehsan Arzaghi [b], Rouzbeh Abbassi [a,*]

[a] School of Engineering, Faculty of Science and Engineering, Macquarie University, Sydney, NSW, Australia
[b] School of Mechanical, Medical and Process Engineering, Faculty of Engineering, Queensland University of Technology, Brisbane, Australia

ARTICLE INFO

Keywords:
Multi-purpose offshore platform
Offshore aquaculture
Wave energy converter
System dynamic
Co-located synergy effect
Reliability modelling

ABSTRACT

In recent years, Multi-purpose Offshore Platforms (MPOP) have emerged as a novel solution to address the increasing global food and energy demand. Beyond the conceptual and qualitative analysis, this paper develops a hybrid quantitative framework to evaluate the life-cycle performance of co-located Wave Energy Converters (WECs) and offshore aquaculture (AQ) systems. The framework integrates hydrodynamic numerical simulations and probabilistic reliability analysis into a System Dynamics (SD) model to simulate complex subsystem interactions and quantify the system productivity and economic feasibility under environmental and operational uncertainty. A case study in Southern Tasmania demonstrates that the upstream WEC farm effectively reduces the incoming wave heights by up to 23%, mitigating aquaculture mooring tensions of the downstream salmon farm by 18%. This protection effect translates into an economic benefit that the co-located configuration achieves a 30.7% reduction in Life Cycle Costs (LCC) compared to the stand-alone configuration. Furthermore, the MPOP demonstrates the robust power capacity, ensuring a continuous off-grid power supply despite long-term component degradation and fluctuating aquaculture power demand. The results validate the MPOP concept as a commercially viable solution for sustainable blue economy development and provide a comprehensive simulation and decision-making tool for exploring future offshore multi-sector cooperation.

Nomenclature

Symbol	Definition	Unit
H_s	Significant wave height	m
T_p	Peak wave period	s
P	Power output	kW
q	WEC farm power efficiency factor	-
k_d	Wave disturbance coefficient	-
R_{tr}	Mooring tension reduction factor	-
C_{LCC}	Life cycle cost	MAUD

1. Introduction

The global demand for food and energy is rapidly increasing due to the growth in human population, which is projected to reach approximately 9.75 billion by 2050. Meeting the resource requirements of this population poses critical challenges in food availability, energy supply, and land use (Ranganathan et al., 2018; Gielen et al., 2019). The International Energy Agency (IEA) reports that the global energy demand increased by 2.2% in 2024, and the Food and Agriculture Organization (FAO) states that global aquatic animal consumption has also reached a new record of 162 million tons in 2024 (Agency, 2025; FAO, 2024). In parallel, environmental degradation driven by greenhouse gas (GHG) emissions intensifies these challenges and underscores the urgency of achieving net-zero emissions by 2050 to limit global temperature rise over 1.5 °C (IEA, 2021). Reaching this target necessitates transitioning the global energy mix towards low-carbon and renewable energy resources, while ensuring a stable and affordable supply. In response, attention has increasingly turned to sustainable engineering solutions that leverage emerging technologies for food production and renewable energy generation, underpinning the shift to a net-zero future (Garavelli et al., 2022).

As land resources for expanding food and energy sectors become constrained, the ocean, which covers 71% of the Earth's surface can offer substantial potential to support sustainable energy production and food security. This idea has been formalised in the concepts of the Blue Economy (BE), which emphasises the use of ocean resources to promote economic growth, while ensuring the health and safety of the

* Corresponding author.
E-mail address: rouzbeh.abbassi@mq.edu.au (R. Abbassi).

https://doi.org/10.1016/j.oceaneng.2026.125210
Received 10 January 2026; Received in revised form 13 March 2026; Accepted 19 March 2026
Available online 27 March 2026

ecosystems (WorldBank, 2017). Within this framework, Marine Renewable Energy (MRE) and offshore aquaculture (AQ) are recognised as two essential sectors that contribute to the BE development. MRE technologies, including waves, tides, currents, as well as offshore wind energy, have been developing rapidly due to their capacity to promote sustainability (Agyekum et al., 2024). Wave energy is outstanding by its ubiquity, high energy density and predictability. Regions such as the Southern Ocean surrounding Australia, where nearshore average wave energy densities reach up to 84 kW/m, represent particularly favourable conditions for energy harvesting (Hemer et al., 2017). Moreover, FAO reported that in 2023, aquaculture production exceeded capture fisheries for the first time, underscoring the ocean's growing role in global food supply. Within the aquaculture industry, salmon farming is an expanding pillar which provides nutrition-rich and high-quality protein to the global population.

Aquaculture operations are increasingly moving further offshore to expand ocean-based production and achieve economies of scale. The exposed offshore environments can also offer improved water quality to enhance fish growth, and enable more effective waste dispersion (Freeman et al., 2022). However, as the distance from shore increases, conventional energy resources for daily operations become less economically viable due to the rising cost of fuel transportation (Menicou and Vassiliou, 2010). Reliance on fossil fuel generators will also continue to impose detrimental environmental impacts. Furthermore, aquaculture assets operating at far-offshore sites are exposed to greater structural loads from harsh environmental conditions. This demands that aquaculture facilities be designed for high reliability, and maintenance plans aimed at achieving high availability, thereby minimising operational risks and costs.

Co-locating offshore MRE facilities with aquaculture facilities offers a competitive solution to the challenges of the offshore aquaculture extension, known as the Multi-Purpose Offshore Platforms (MPOPs) (Griffin et al., 2015; EuropeanUnion, 2014). This concept enables to create synergy through both functional integration and spatial proximity. Offshore renewable energy technologies can replace traditional fossil fuel generators used in aquaculture operations, reducing carbon emissions and lowering fuel transportation costs. Meanwhile, a co-locating configuration can be designed strategically to improve system structural and operational reliability. For instance, Silva et al. (Silva et al., 2018) suggest that a Wave Energy Converter (WEC) farm can act as a shelter and protect downstream fish cages from heavy wave loads, reducing the risks of structural failure.

As for the aquaculture sector, despite the growing interest in offshore operation, most studies still focus on nearshore and coastal activities (Crawford et al., 2002; Fløysand et al., 2020; Meng et al., 2022). Recent research has evaluated the site suitability for offshore fish farms by extrapolating the extreme wave events in the potential area from historical wave data (Ma et al., 2025). However, few studies investigate the actual wave loads acting on the fish cages or the reliability of aquaculture structures operating under offshore conditions.

MPOP design further increases the system's complexity. Integrating multiple systems means their interactions must be considered explicitly, and this added complexity introduces more uncertain parameters that affect both the performance of each subsystem and the overall behaviour of the integrated system. Current MPOP designs remain largely conceptual or at the prototype stage. Previous research has assessed the feasibility of offshore MPOPs and identified critical environmental, economic, and reliability considerations (Abhinav et al., 2020; Aryai et al., 2021), but these studies provide only qualitative assessments of operational uncertainty and risk. Although several studies have examined how much wave height reduction can be achieved by an upstream WEC farm (Silva et al., 2018; Verao Fernandez et al., 2021), the resulting reduction in hydrodynamic loads on the downstream aquaculture farm, and the associated reduction in structural failure and system operational cost, remain unknown. Therefore, a major gap is the absence of a study that advances beyond preliminary design of the MPOP to quantitatively evaluate interaction effects and life-cycle performance of the system under operational uncertainties. Key performance indicators, including renewable energy generation, aquaculture productivity, structural reliability and life-cycle cost, need to be evaluated together to represent the realities of co-located system operation. Additionally, as the offshore environment and ocean ecosystem change continuously over time, which introduce additional uncertainties. Traditional static analytical approaches are insufficient, therefore, dynamic tools are needed to model trade-offs and interactions while incorporating temporal feedback in MPOP systems (Geary et al., 2020). Turschwell et al. (Turschwell et al., 2022) also emphasise the need to address multi-sector interactions across the life-cycle of offshore sectors to ensure sustainable ocean use.

To address these gaps, this study presents a System Dynamics (SD) model, supported by numerical simulations, to evaluate the performance of a co-located WEC and aquaculture system, in terms of power generation, food production and life-cycle cost under uncertain offshore environmental conditions. The model evaluates the feasibility of using wave energy to power aquaculture facilities and to provide structural protection by reducing wave loads on the downstream fish cages. The reliability aspects of the WEC farm are incorporated to estimate the expected power availability and to assess the economic viability of offshore system co-location. This integrated approach captures subsystem interactions, operational uncertainties, and key design considerations for future MPOP design, and supports informed decision-making for offshore renewable energy and aquaculture stakeholders in further development and collaboration.

2. Methodology

This section presents the developed methodology, which aims to comprehensively evaluate the performance of co-located MPOPs, integrating wave energy and offshore aquaculture systems. Three key performance indicators are dynamically simulated, including energy production, aquaculture system productivity, and life-cycle costs. These indicators are assessed considering uncertainty in environmental conditions and system operation using a SD modelling approach.

As illustrated in the flowchart (Fig. 1), the methodology is structured into four main stages. First, the plausible MPOP design and site selection are established based on literature review and environmental suitability assessment. Then, the coupled hydrodynamic and wave propagation simulations are performed to quantify the near-field and far-field hydrodynamic characteristics of the WEC farm. This includes evaluating energy production, quantifying the wave shadowing effect, and determining the resulting wave loads on the downstream aquaculture system protected by the WEC farm. Third, these physical responses are processed through probabilistic reliability modelling to derive sea-state-specific failure probabilities for both WEC and aquaculture facilities. Finally, all these results are integrated into a SD model, which simulates MPOP system operations under uncertain environmental conditions and quantifies the overall techno-economic performance. The detailed description of each stage along with the associated mathematical formulations are introduced in the following sections.

2.1. MPOP design

2.1.1. Aquaculture farm

In this paper, offshore salmon farms are selected as the representative of aquaculture systems, as it is the cornerstone of the Australian aquaculture industry with significant potential for offshore expansion (Freeman et al., 2022). Circular gravity-based open net cages are chosen for performance assessment. This technology is widely adopted by the industry and has proven application in diverse marine conditions (Shen et al., 2018). As shown in Fig. 3, each array considered in this study consists of six cages arranged in a 2×3 configuration.

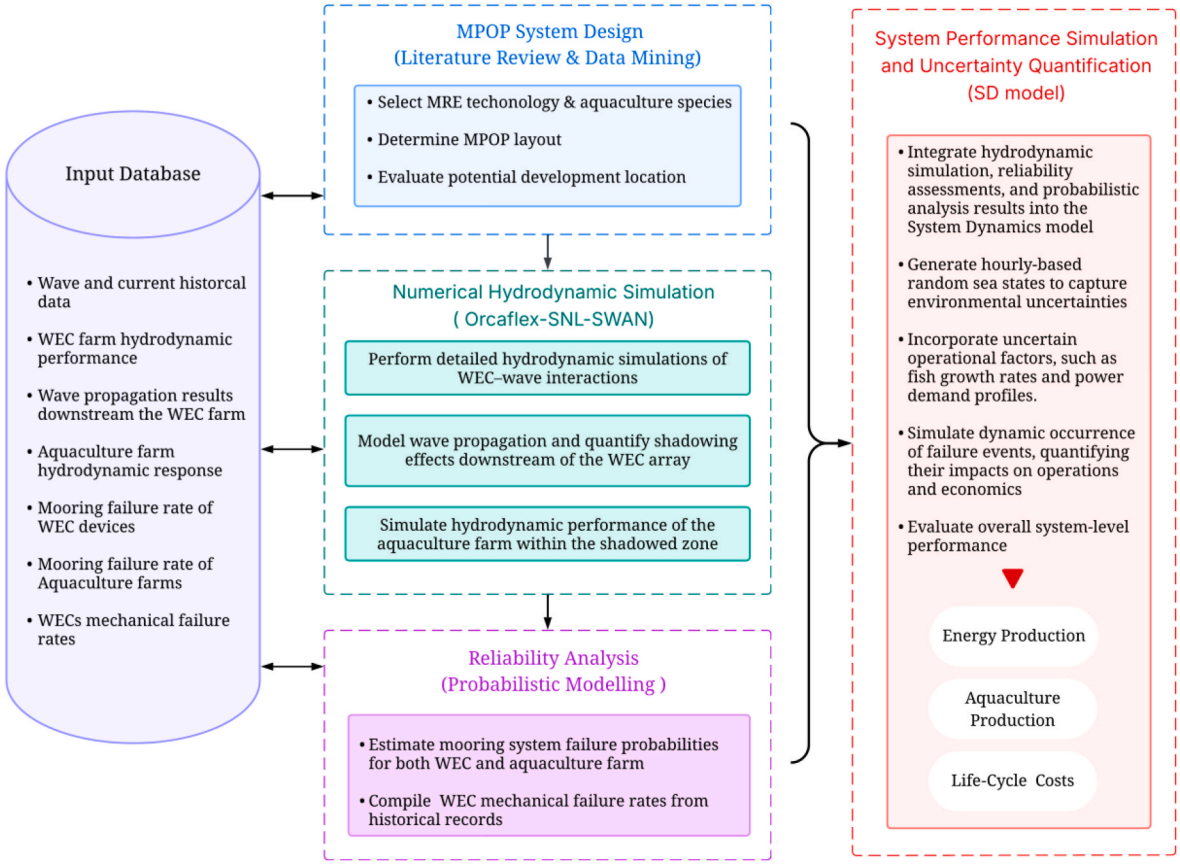

Fig. 1. Developed framework for system dynamics modelling of Multi-purpose Offshore Platform (MPOP).

2.1.2. *WEC technology*

In this study, a fully submerged three-tether point-absorber WEC is selected as a suitable technology for MPOP development. This was adopted from the novel *CETO 6* concept, owing to its maturity in development (Carnegie). The submerged design improves survivability compared to surface-floating WECs, ensuring continuous energy extraction during harsh sea conditions.

As illustrated in Fig. 2, the WEC consists of a large flat cylindrical buoy connected to three individual power take-off (PTO) systems, each integrated with inclined taut mooring lines. The PTO is essentially a belt-driven pulley system that enables the conversion of wave-induced buoy motion into electrical energy. Additionally, the three-tether design allows energy capture from multiple degrees-of-freedom (DOFs) of the buoy motion. This configuration provides higher energy conversion efficiency than conventional heave-based point absorber devices, which predominantly capture energy from vertical motion (Orszaghova et al., 2020).

2.1.3. *Co-location design*

As discussed before, co-locating a WEC farm with an aquaculture farm forms the basis of the MPOP design. This integration is critical in supporting the sustainable development of offshore aquaculture, simultaneously addressing energy supply and structural integrity challenges. The WEC farm powers the aquaculture operations, while protecting the downstream structures.

Fig. 2. Three-tethered submerged Wave Energy Converter (WEC).

For the WEC device orientation, the study follows the recommendations of Bao et al. (Bao et al., 2024a), where the predominant wave direction acts perpendicular to the axis connecting two anchor points, rather than being aligned with an individual tether. This configuration has been proven to distribute wave loads on the tethers effectively, balancing energy generation and structural integrity.

As shown in Fig. 3, this paper adopts an arrow farm layout configuration based on the findings of López-Ruiz et al. (López-Ruiz et al., 2018). In comparison with the staggered and aligned layouts considered in their investigation, the arrow arrangement demonstrated minimal interference amongst WECs, thus offering superior power extraction capacity. Additionally, the arrow configuration enhances availability by improving access for inspection and maintenance, which reduces disturbance to other operating WECs while repair is being undertaken. A disadvantage of this layout is its large footprint, potentially resulting in inefficient space utilisation, however, locating the aquaculture farm within the downstream shadow zone can mitigate this limitation by providing a synergistic use of space.

Fig. 3 illustrates a schematic of the MPOP layout where the size or capacity of each subsystem can be altered based on the application.

2.2. *MPOP implementation location*

2.2.1. *Development site selection*

Given the high costs associated with connection to the grid at long-distance offshore locations, this study adopts an off-grid system configuration design which aims to supply the power demand of

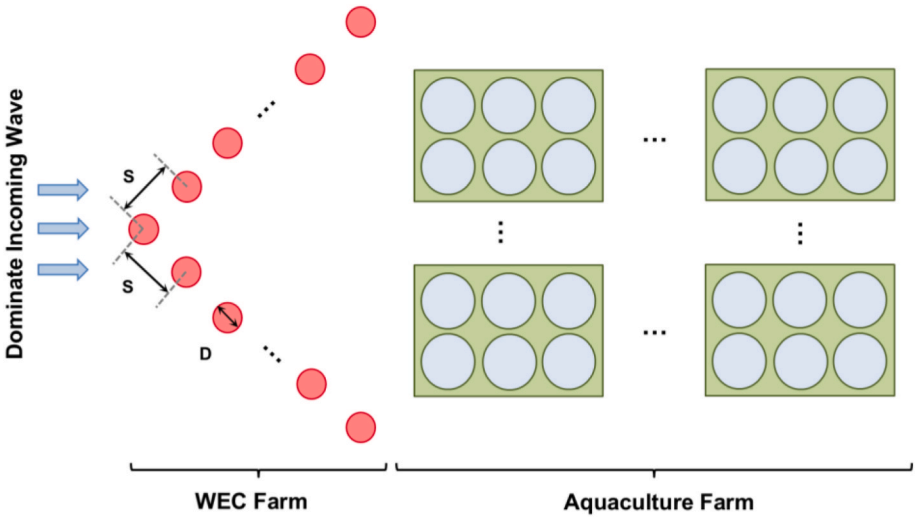

Fig. 3. Schematic layout of the designed MPOP for WEC and aquaculture system integration.

aquaculture operations directly by the WEC systems. Diesel generators are considered as the backup energy source to cover unexpected power shortage (Syse, 2016). As a result, the presence of sufficient harvestable wave energy corresponding to the size of the WEC farm is an important criterion in selecting the MPOP site.

Site selection for a co-located MPOP will also focus on utilising mature coastal aquaculture systems that are readily transferable to offshore. That is, plausible designs are taken from proven coastal operations to further points in the sea where more energy is available for harvesting and to leverage established practices and infrastructure, while minimising transport and installation demands.

2.2.2. Site environmental modelling

To reliably evaluate the operational performance of an MPOP, it is essential to consider long-term sea state variations at the selected deployment site. In this paper, a 20-year historical dataset encompassing significant wave height (H_s), wave period (T_p) and wave direction data is collected from the Wave Energy Atlas ("National Map).

The joint probability distribution of wave height and wave period is constructed, and representative sea states are established using the k-means clustering algorithm. This method divides the large dataset into a predefined number of clusters, with centroids are characterised by mean H_s and T_z values (Lavelle and Kofoed, 2013). According to Sergiienko et al. (Sergiienko et al., 2021), the occurrence probability of each selected wave condition is calculated by summing the probabilities of the data points within the corresponding cluster. Additionally, recorded wave directions are discretised into eight primary directional sectors (N, NE, E, SE, S, SW, W and NW) to reflect wave directional variability at the site. Wave direction probabilities are computed by dividing occurrences from each direction by the total counts of waves.

For subsequent numerical simulation, irregular wave conditions are generated from the identified sea states using the Joint North Sea Wave Project (JONSWAP) spectrum, which is extensively employed and validated within wave energy research (Prendergast et al., 2018). The spectral density $S(f)$ is expressed in Eq. (1) (Bao et al., 2024b):

$$S(f) = \frac{\alpha g^2}{16\pi^4} f^{-5} \exp\left[-\frac{5}{4}\left(\frac{f}{f_p}\right)^{-4}\right] \gamma^{\exp\left[-\frac{(f-f_p)^2}{2\sigma^2 f_p^2}\right]} \tag{1}$$

Where f is wave frequency, g denotes the acceleration due to gravity, f_p is the peak wave frequency, α is intensity of the spectrum, σ is the spectral width parameter and γ is the peak enhancement factor (Guo and Xu, 2011).

2.3. WEC near-field hydrodynamics

In this study, Orcaflex, a time-domain linear potential flow solver is selected to model and simulate the hydrodynamic characteristics and mooring behaviour of single WEC devices. The capability and accuracy of this numerical package have been validated in prior WEC research. Rosenberg et al. (Rosenberg et al., 2019) demonstrated the effectiveness of Orcaflex in predicting the WEC design loads under the irregular wave conditions, and Paduano et al. (Paduano et al., 2020) validated Orcaflex simulation results against experimental data, highlighting its accuracy in predicting mooring system loads for floating offshore structures.

The general governing equation solved by Orcaflex in the time domain is expressed by Eq. (2) (Orcaflex):

$$M(p,a) + C(p,v) + K(p) = F(p,v,t) \tag{2}$$

where $M(p,a)$ is the system inertia force, $C(p,v)$ is the system damping force, $K(p)$ is the system stiffness force, and $F(p,v,t)$ is the external force. Parameters p, v, a are the position, velocity, and acceleration vectors, respectively, and t is the simulation time.

For the WEC-wave interaction simulation, the numerical modelling and simulation setup have been detailed introduced in the previous research, including the numerical representation of the PTO and mooring system as well as their nonlinear parametric settings (Bao et al., 2024b). Power production for the single WEC device is computed by summing the power extracted by the WEC three separate PTO systems based on the simulation results.

2.4. WEC far-field hydrodynamics

Assessment of WEC farm performance requires resolving both device hydrodynamics and its impact on the surrounding wave field. Since single-device estimates are not accurate in characterizing array interactions, wake effects, and directional spreading inside the farm. The numerical model discussed in the previous section provides structural response and absorbed power of each WEC device under specific sea states. These outcomes must be expanded into a WEC array representation within a wave-propagation model (López-Ruiz et al., 2018; Rijnsdorp et al., 2020). This captures the transportation of wave energy through the array and into the downstream area, giving consistent estimates of in-farm interaction and shadowing.

2.4.1. Wave propagation simulation

To simulate the wave propagation passing the WEC farm, this study employs the spectral wave model Simulating Waves Nearshore (SWAN).

This package is widely employed for assessing WEC farm shadowing effects. For example, Onea and Rusu (2019) simulated 24 WECs in an aligned arrangement using the SWAN, reporting up to 41% wave-height reduction in the lee of the WEC farm. In SWAN, the wave propagation is governed by the universal wave action balance equation, expressed by Eq. (3):

$$\frac{\partial N}{\partial t}+\nabla_{\vec{x}}\cdot\left[\left(\vec{c}_g+\vec{u}\right)N\right]+\frac{\partial c_\sigma N}{\partial \sigma}+\frac{\partial c_\theta N}{\partial \theta}=\frac{S_{\text{tot}}}{\sigma} \tag{3}$$

where $N(\vec{x},t;\sigma,\theta)=\frac{E}{\sigma}$ represents the wave action density ($\vec{x}$ is the spatial coordinate, t is time, θ denotes the wave direction, E is the wave energy density and σ is the wave frequency). $\nabla_{\vec{x}}$ is the horizontal spatial gradient operator. $\vec{c}_g$ and $\vec{u}$ represent wave group velocity and ambient current speed, respectively. c_σ and c_θ represent the rate of change in wave direction and wave frequency respectively. S_{tot} represents the total energy source, which accounts for wave generation, dissipation, boom friction and wave breaking.

Standard SWAN set-ups theoretically represent the WEC power absorption with a constant transmission coefficient (k_t) (Verao Fernandez et al., 2021). However, in reality, though WEC power capacity is highly frequency-dependent. Stokes and Conley (2018) demonstrate that using a constant k_t introduces large uncertainty, estimating that downstream wave energy reduction varies from 4% to 44%. To address this limitation, Sandia National Laboratory SWAN (SNL-SWAN) package is adopted in this study(Ruehl et al., 2013). Unlike the conventional SWAN, this modified model allows the calculation a frequency-dependent transmission coefficient based on the specific WEC power matrix (parameterised by H_s and T_p).

Within the model, the squared power transmission coefficient (k_t^2) is defined as the ratio of absorbed power (P_{Absorbed}) to incident wave power (P_{Incident}), as expressed in Eq. (4). During the simulation, the model continuously identifies the local wave height and period at the WEC location, looks up the input matrix to determine the exact power absorbed under those specific conditions and updates the transmission coefficient dynamically.

$$k_t^2=\frac{P_{\text{Lee}}}{P_{\text{Incident}}}=\frac{P_{\text{Incident}}-P_{\text{Absorbed}}}{P_{\text{Incident}}}=1-\frac{P_{\text{Absorbed}}}{P_{\text{Incident}}} \tag{4}$$

The accuracy of the SNL-SWAN simulation relies on the precision of the input power matrix, which necessitates the simulation of a single WEC device hydrodynamic performance. Thus, this study couples the OrcaFlex with SNL-SWAN (here named as OrcaFlex–SNL-SWAN approach). OrcaFlex is used to simulate the complex near-field hydrodynamics of the CETO 6 device, providing device-level power extraction, which is mapped into the SNL-SWAN required power matrix, for estimation of WEC farm shadowing effect.

The resulting downstream wave-height reduction induced by the WEC farm is characterised by the disturbance coefficient k_d, defined as the ratio of the downstream wave height (H_{Lee}) to the incident wave height (H_{Incident}), given by Eq. (5):

$$k_d=\frac{H_{\text{Lee}}}{H_{\text{Incident}}} \tag{5}$$

2.4.2. Power production of WEC farm

The farm-scale power output depends on both individual performance and hydrodynamic interactions within the array. Upstream devices absorb a large portion of the incident wave energy, creating a shadowed zone of reduced energy flux available to downstream devices.

In this study, the OrcaFlex-derived power matrix is imported into SNL-SWAN, so the incident wave spectrum is propagated through the WEC farm and the local energy flux at each device location is resolved. The total power output of the farm is the summation of the extracted power from individual devices, given by Eq. (6):

$$P_{\text{Farm},ij}=\sum_{k=1}^{n_{\text{WEC}}}P^k_{\text{WEC},ij} \tag{6}$$

where $P^k_{\text{WEC},ij}$, is the power generated by the k th WEC in the farm under wave condition$i$ and wave direction j. n_{WEC} is the number of devices in the array.

The expected long-term farm power output is evaluated by integrating these power outputs across the joint probability distribution of the operational site environmental conditions. Farm power generation from each sea state is multiplied by its probability of occurrence and then summed over all states, expressed in Eq. (7):

$$E[P_{\text{Farm}}]=\sum_{j=1}^{m}\sum_{i=1}^{n}P_{\text{Farm},ij}\cdot p_i\cdot p_j \tag{7}$$

Where p_i and p_j are the occurrence probability of the i^{th} sea-state and j^{th} wave direction respectively. In practice, the expected long-term farm power output is evaluated over discrete sea-state and directional bins using the joint probability distribution of occurrence, as shown by Eq. (7). Conceptually, this can be represented in continuous form as an integral over the wave-condition space.

To quantify array-interaction effects on power extraction, the WEC farm efficiency factor (q-factor) is used, calculated by Eq. (8):

$$q=\frac{P_{\text{Farm}}}{n_{\text{WEC}}\cdot P_{\text{Isolate}}} \tag{8}$$

Where P_{Farm} is the simulated farm power output, P_{Isolate} is the power output of single, stand-alone WEC. The q-factor values near 1 indicate negligible interaction losses, while values below 1 quantify the reduction in total energy generation caused by WECs interactions within the array.

2.5. Aquaculture system hydrodynamic analysis

This study quantifies the protective effect of the upstream WEC array on the structural integrity of downstream aquaculture systems using time-domain numerical modelling based on the lumped-mass formulation. The numerical simulations of the fish farm array were conducted to evaluate the hydrodynamic loads on flexible net cage structures under realistic combined wave-current conditions. This approach follows the recommendations of Shen et al. (Shen et al., 2018) and Tang et al. (Tang et al., 2020), whose studies confirmed that combined environmental loading produces significantly larger hydrodynamic forces on aquaculture farms compared to wave-only or current-only scenarios.

Based on a detailed literature search, the anchoring system was identified as the most critical determinant of structural reliability and operational safety for offshore fish farms (Tang et al., 2020; Cifuentes Salazar, 2016). For this reason, this study focused on the analysis of failures in mooring lines of the aquaculture farm to measure the protective benefit of the co-locating MPOP. Mooring-line tensions were obtained from the numerical simulations and compared across two scenarios: one without upstream WEC protection, exposing the aquaculture cages to offshore waves and current, and another with wave-height reduction provided by the upstream WEC farm.

To quantify the shadowing effect on anchor-line tension, the tension reduction factor (R_{tr}) is introduced, representing the ratio of the fish farm mooring line tension with co-located WEC farm protection ($T_{\text{Protected}}$) to that of stand-alone system ($T_{\text{stand-alone}}$), given by Eq. (9):

$$R_{tr}=\frac{T_{\text{Protected}}}{T_{\text{stand-alone}}} \tag{9}$$

For the protected scenario, the shadowed downstream sea-state is identified by scaling the incident wave height by the k_d value derived from the wave propagation modelled, expressed by Eq. (5). Wave

periods remain unchanged within the shadowed zone because of the wave propagation theory applied in SNL-SWAN (Ruehl et al., 2013). Energy extraction by the devices is estimated by considering a reduction in spectral energy density during propagation while the linear dispersion relation is preserved, so the spectral peak period does not change. In other words, absorption lowers the energy spectrum magnitude without changing its frequency distribution. Additionally, ambient currents are represented using a standard power-law profile to capture typical offshore vertical velocity gradients.

2.5.1. Aquaculture farm hydrodynamic simulation

In OrcaFlex, the lumped-mass approach is used to simulate line structures. The *line* element is discretised into a series of massless segments connected by nodes located at segment ends. These segments carry structural properties such as axial and torsional stiffness, while structural mass, buoyancy, and hydrodynamic loads are lumped at the nodes. Consequently, each node accumulates contributions from the two connected segments. The governing equation of motion for each node is expressed by Eq. (10) (Niosi et al., 2023):

$$M_n\ddot{x}_n(t) = T_{n+1}(t) - T_n(t) + F_{C,n+1}(t) - F_{C,n}(t) + F_{B,n}(t) + F_{D,n}(t) + F_{G,n}(t) + F_{ext,n}(t) \tag{10}$$

where M_n represents the lumped mass at node n, including structural mass and added mass accounting for inertia effects. $\ddot{x}_n(t)$ is the node acceleration. $T_{n+1}(t)$ and $T_n(t)$ are the axial tension from adjacent segments of node n. Similarly, $F_{C,n+1}(t)$ and $F_{C,n}(t)$ denote the damping forces in the adjacent segments. $F_{B,n}(t)$ and $F_{G,n}(t)$ are the buoyancy and gravity forces at the node, respectively. $F_{D,n}(t)$ accounts for hydrodynamic drag force and $F_{ext,n}(t)$ is the external forces, such as those caused by interactions with the seabed or other structural components.

To determine the drag force and the inertia effects required in Eq. (10), the hydrodynamic load on the *line* elements is computed using Morison's equation. The general form used in the numerical simulation is given by Eq. (11) (Orcina, 2016):

$$F_w(t) = \frac{1}{2}\rho C_d d_{seg} L_{seg} |v(t) - u(t)|[v(t) - u(t)] + \rho C_M \frac{\pi}{4} {d_{seg}}^2 L_{seg} \dot{v}(t) - \rho(C_M - 1)\frac{\pi}{4}{d_{seg}}^2 L_{seg}\dot{u}(t) \tag{11}$$

where $F_w(t)$ is the total hydrodynamic force on the segment. d_{seg} and L_{seg} represent the segment diameter and length, respectively. C_d and C_M are drag and inertia coefficients. $u(t)$, $v(t)$, $\dot{u}(t)$, and $\dot{v}(t)$ are segment and fluid velocities and segment and fluid accelerations, respectively.

For slender netting elements with small twine diameters, inertial forces are negligible. Thus Eq. (11) is simplified into normal drag force($F_{D,nor}$) and the tangential drag force($F_{D,tan}$) components, shown in Eqs. (12) and (13):

$$F_{D,nor} = \frac{1}{2}\rho d_{seg} L_{seg} C_{d,n}(v_{r,n})|v_{r,n}| \tag{12}$$

$$F_{D,tan} = \frac{1}{2}\rho d_{seg} L_{seg} C_{d,t}(v_{r,t})|v_{r,t}| \tag{13}$$

Where the $C_{d,n}$, and $C_{d,t}$ are the normal and tangential drag coefficients, respectively. $v_{r,n}$ and $v_{r,t}$ denote relative velocity between fluid and net twine segment in normal and tangential directions, respectively.

2.5.2. Aquaculture farm numerical modelling

The complex geometry of the aquaculture farm is modelled by *line* elements and are joined using *buoys* in Orcaflex. Floating collars and sinker tubes are modelled as homogeneous pipes (line elements with applied bending stiffness), joined by 6-degree-of-freedom (6D) buoys to capture rigid body motions. In contrast, the flexible net twines are modelled as ropes (line elements with negligible bending stiffness) connected by 3-degree-of-freedom (3D) buoys. To represent structural connection without introducing additional physical properties, these specific 3D buoys are assigned negligible volume, and their hydrodynamic coefficients are set to zero.

Due to the impracticality of modelling every physical twine, an equivalent net model is developed. This approach groups multiple physical twines into a single numerical twine, while preserving the global hydrodynamic properties of the net cage. The equivalence is achieved by matching key physical properties: solidity, wet mass, and axial stiffness (Cifuentes Salazar, 2016).

To maintain identical solidity the numerical twine diameter (d_n) and length (L_n) are adjusted based on the physical cages twine diameter (d_p) and length (L_p), given in Eq. (14):

$$\sum(d_p \cdot L_p) = \sum(d_n \cdot L_n) \tag{14}$$

The mass of the 3D buoys (M_n^{wet}) is adjusted to precisely match the wet mass of the physical net (M_p^{wet}), as given by using Eq. (15):

$$M_p^{\text{wet}} = W_p - B_p = M_n^{\text{wet}} = W_n - B_n \tag{15}$$

Where W and B denote the weight and buoyancy, respectively. The axial stiffness of the equivalent line element is determined to match the sum of the axial stiffness of the corresponding physical twine groups, as given by Eq. (16):

$$E_n A_n = n_{\text{twine}} \cdot E_p A_p \tag{16}$$

Where E is Young's modulus, A is the line element cross-sectional area, and n_{twine} is the number of physical twines represented by one numerical line element.

2.6. MPOP reliability analysis

This study adopts a systems engineering approach to investigating the reliability of the MPOP, recognising that the structural integrity of WEC devices and aquaculture system influences energy production, aquaculture productivity, and life-cycle costs. For the reliability assessment, failure modes, failure rates, and severities for the WEC devices are taken from established point-absorber reliability databases. Failure modes are classified into three severity levels: minor failures (mf), major failures (Mf), and critical failures (Cf). Minor and major failures represent those events that result in system availability degradation with no major downtime interrupting energy production. Their failure rates are therefore used to calculate an overall availability for the WEC farm.

The availability of the WEC farm (A) at operation time t is calculated using the minor and major failure rates ($\lambda_{m\&M}$), and the corresponding repair rates ($\mu_{m\&M}$), expressed by Eq. (17):

$$A(t) = \frac{\mu_{m\&M}}{\lambda_{m\&M} + \mu_{m\&M}} + \frac{\lambda_{m\&M}}{\lambda_{m\&M} + \mu_{m\&M}} e^{-(\lambda_{m\&M} + \mu_{m\&M})t} \tag{17}$$

In contrast, critical failures require offshore repair interventions, resulting in substantial downtime, power generation losses, and increased unplanned maintenance costs. It is recognised that the mooring configurations of specific technologies may differ from generic point-absorber set-ups, which may lead to deviations in their reliability characteristics compared with those derived from published mooring failure rates. Numerical simulations are therefore conducted to evaluate mooring tensions under combined wave and current loading conditions. The same rationale can be applied to aquaculture assets, where mooring failures are considered as the most critical events during operation. Failure due to extreme load, here represented by the ultimate limit state (ULS), and fatigue failure are considered for mooring system reliability assessment in this paper. The employed method for assessing the probability of failure follows previous research by Bao et al. (2024a),

extended here to evaluate the mooring reliability of both WEC devices and downstream aquaculture array.

For ULS assessment, the Peak-over-Threshold (POT) method is used to predict extreme mooring tension occurrences over the operational lifetime. The Generalized Pareto Distribution (GPD) is fitted to tension peaks exceeding a threshold defined by the mooring line Ultimate Tensile Strength (UTS) (ABS, 2012). A failure event is recorded when predicted extreme tensions exceed this minimum breaking load (MBL).

For fatigue assessment, failure occurrence is predicted using the rainflow counting (RFC) combined with the S-N curve approach. Stress cycles filtered through RFC are evaluated using the Palmgren-Miner linear damage accumulation rule, whereby the time-varying cumulative fatigue damage $D(t)$ is calculated using Eq. (18) (Brodtkorb et al., 2000):

$$D(t) = \sum_{t_k \le t} \frac{1}{N(s_k)} \tag{18}$$

Where s_k is the filtered stress range of k^{th} cycle. $N(s_k)$ denotes the number of cycle-to-failure corresponding to s_k, predicted by the S-N curve. Fatigue failure is considered to occur when the accumulated damage reaches unity.

2.7. MPOP system dynamic model

This study develops a comprehensive SD model to evaluate the life-cycle performance and synergistic effect of the co-located WEC and offshore aquaculture systems, explicitly addressing uncertainties associated with environmental and operational conditions. This SD model incorporates outcomes from detailed numerical simulations, including WEC farm power generation capacity and its shadowing effects in reducing hydrodynamic loads on downstream aquaculture structures. Reliability assessments derived from statistical analyses and probabilistic modelling of the simulation outputs are then incorporated to estimate WEC farm availability degradation, expected system output and potential failure consequences.

Within the SD model, the system life-cycle is simulated using hourly time steps over a 20-year operational period that captures temporal variations in key model parameters. Three performance indicators including energy production, aquaculture productivity and life-cycle cost are modelled as *stock* variables, so that their variation is represented consistently across the MPOP life-cycle. Multiple scenarios have been developed to analyse system performance under alternative operational and environmental conditions. The detailed SD modelling methodology is discussed in the following sections.

2.7.1. Food production of aquaculture farm

The total fish biomass is a critical system variable, as it determines the food production and the revenue stream of the MPOP. The total biomass of fish in the aquaculture system (S_{fish}) is computed by integrating the fish growth rate and subtracting the fish mortality and harvest rates. This relationship is expressed in Eq. (19):

$$\frac{dS_{fish}}{dt} = G_{AQ}(t) - D_{AQ}(t) - H_{AQ}(t) \tag{19}$$

Where $G_{AQ}(t)$, $D_{AQ}(t)$, and $H_{AQ}(t)$ represent the salmon growth rate, mortality rate, and harvest rates, respectively. To capture the inherent biological uncertainty in aquaculture operations, variability is introduced into these parameters. In the developed SD model, presented in Fig. 4, the specific growth and mortality rates for each farming stage are sampled from fluctuating ranges rather than being fixed values based on the latest aquaculture industry reports.

2.7.2. Energy flow in MPOP

As the energy strategy of MPOP is self-sufficiency, the WEC farm supplies the immediate power demand of the aquaculture operations, with any surplus energy used for auxiliary systems or stored. The cumulative energy stock of the system (E_{net}) is given by Eq. (20):

$$\frac{dE_{net}}{dt} = N_{WEC}(t) \times P_{WEC}(t) \times q \times A(t) - P_{AQ}(t) \tag{20}$$

Where $N_{wec}(t)$ represents the number of operating WEC in the farm. $P_{AQ}(t)$ denotes the instantaneous power demand of the aquaculture farm at the operational time t. q is the farm efficiency factor (q-factor) and $A(t)$ denotes the WEC farm availability. A positive energy flow rate $\frac{dE_{net}}{dt} > 0$ indicates that the WEC farm provides surplus energy to power the aquaculture system. Conversely, a negative value signifies an energy shortfall, necessitating supplemental power from backup generators or energy storage systems to sustain aquaculture operations.

The SD model representing the energy flow within the MPOP system is shown in Fig. 5. At each time step, the model generates a random sea state (defined by wave height, period, and direction) based on the

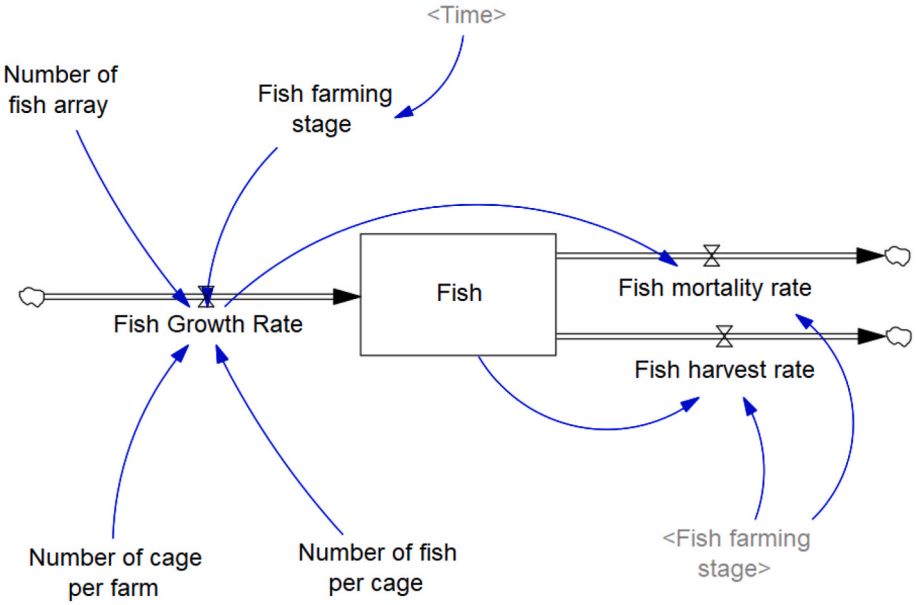

Fig. 4. Developed System Dynamic (SD) model for system food production.

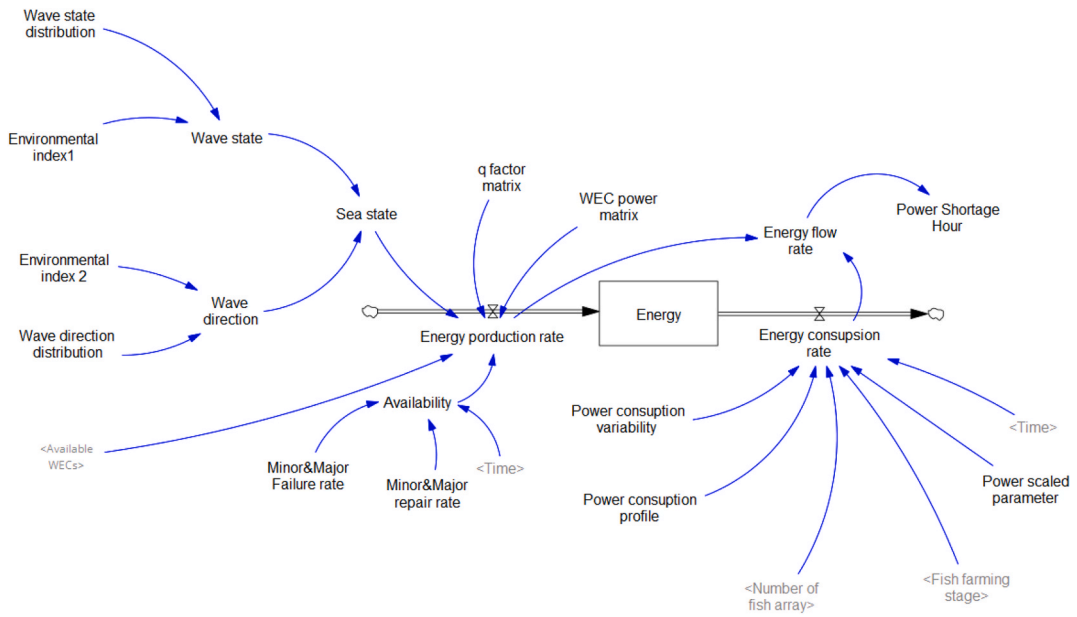

Fig. 5. Developed SD model for system energy flow.

occurrence probabilities derived from the environmental modelling (Section 2.2.2). In the SD model, these probabilities are represented in the *Environmental Index* variable. This index is then used to query a lookup table adopted from the hydrodynamic simulation results (Section 2.4), mapping the generated environmental condition to its corresponding expected WEC power capacity and farm efficiency factor.

2.7.3. Critical failure event modelling of MPOP

Critical failure events of both the WEC farm and the aquaculture farm are simulated within the SD model. For the WEC farm, the simulated events include mechanical failures due to severe structural damage of the buoy and PTO components, mooring ULS failures and mooring fatigue failures. As illustrated in Fig. 6, the number of operational WECs in the farm is tracked by a discrete integer stock. The stock changes only when critical failure or repair events occur. The relationship governing the number of available WEC (n_{Avail}) is expressed by Eq. (21):

$$n_{\text{Avail}}(t) = n_{WEC}(t-\Delta t) - n_{CF}(t) + n_{CR}(t) \tag{21}$$

where $n_{CF}(t)$ is the number of WEC units down because of critical failures at time t, and $n_{CR}(t)$ represent the number of the WEC that have been repaired.

Assuming a constant arrival rate for mechanical failures, the number of failures (k) is modelled using Poisson distribution in a SD model, given by Eq. (22):

$$P(X=k) = \frac{(\lambda_c \cdot t)^k e^{-(\lambda_c t)}}{k!} \tag{22}$$

Where λ_c denotes the mechanical critical failure rate of WEC.

In the SD model, the occurrence of mooring failures at each hourly time step t is determined based on the uncertain environmental conditions generated at that step. For the ULS mooring failures, the model retrieves the corresponding failure probability under the generated sea state using the POT approach. Then, a random variable, uniformly distributed between 0 and 1, is generated, and a failure event is recorded if this value falls below the failure probability threshold.

Simultaneously, the model tracks the mooring fatigue failure by calculating the hourly accumulated fatigue damage specific to the sea state and adding it to a cumulative damage stock variable. A fatigue failure event is triggered when this accumulated damage reaches unity. When either a ULS or fatigue mooring failure is identified, the WEC is removed from the available WECs stock, and a repair process is initiated using delays based on the mean time to repair (MTTR), after which the

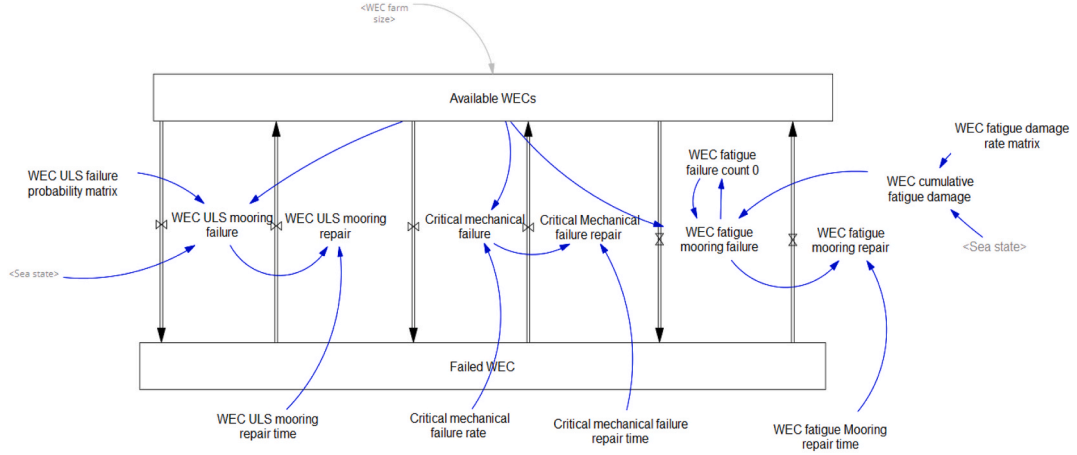

Fig. 6. Developed SD model for number of available WEC in system.

component returns to operation and contribute to farm-level energy production.

Similarly, critical mooring failures for the aquaculture system are also simulated in the SD model. When simulating co-located scenarios, the tension reduction factor (R_{TR}) is applied to adjust mooring tensions. This adjustment is to reflect reduced hydrodynamic loads due to the wave shadowing effect of the WEC array, subsequently influencing the frequency of mooring failures and related corrective maintenance activities in the aquaculture system. In reality, other localised failure modes, such as net twines breakage or floating collar cracking, may occur. However, under combined offshore wave and current loading conditions, mooring lines represent the most critical components that govern the overall system station-keeping and structural integrity. Therefore, this study adopts these critical mooring failures as key structural reliability indicators for the aquaculture system.

2.7.4. Life-cycle cost modelling of MPOP

The economic viability of the MPOP depends on a critical trade-off between energy production revenue, aquaculture productivity, and the costs associated with system reliability. To quantify this, the study develops a Life Cycle Cost (LCC) model that simulates the total expenditure associated with routine operations and uncertain failure events over the project lifespan. The LCC is modelled as a stock variable within the SD framework, shown in Fig. 7.

The LCC (C_{LCC}) of the MPOP system is calculated by summing of capital expenditure (C_{CAPEX}), operational expenditure (C_{OPEX}), and decommissioning expenditure (C_{DECOM}) with the consideration of the annual discount rate, given by Eq. (23):

$$C_{LCC}(t) = C_{CAPEX} + \sum_{\tau=0}^{t} \frac{C_{OPEX}(\tau)}{(1+r)^{\frac{\tau}{8760}}} + \mathrm{I}(t = T_{end}) \cdot \frac{C_{DECOM}}{(1+r)^{T_{end}}} \tag{23}$$

Where t is the simulation time in hour. $C_{OPEX}(\tau)$ represent the instantaneous operational cost. r denotes the annual discount rate. This rate is applied to account for the time value of money, ensuring the future operational and decommissioning costs are appropriately discounted to their present value to accurately model the system LCC. The C_{DECOM} is added into the LCC stock only when the simulation reaches the end of the project life stock (T_{end}), by applying the indicator function I($t = T_{end}$).

While C_{CAPEX} and C_{DECOM} are fixed costs that are spent at the beginning and end of the project life-cycle, this paper focuses on C_{OPEX} to evaluate the effect of uncertainty in operational conditions on project costs. This comprises the fixed routine operational costs (C_O) and maintenance costs (C_M), as expressed by Eq. (24):

$$C_{OPEX}(t) = C_O + C_M(t) \tag{24}$$

The C_M is treated as an event-driven variable, given in Eq. (25). This includes the cost of scheduled preventive maintenance (C_{PM}) and uncertain corrective maintenance (C_{CM}). The expenditure is triggered only upon the completion of specific maintenance activities.

$$C_M(t) = C_{PM}(t) + C_{CM}(t) \tag{25}$$

Preventive Maintenance (PM) events follow a fixed schedule at a fix rate of $C_{PM,system}$. In the SD model, this is modelled as a discrete inflow that occurs at fixed intervals, as described in conditional function Eq. (26):

$$C_{PM}(t) = \begin{cases} C_{PM,system} & \text{if preventive maintenance is completed at } t \\ 0 & \text{otherwise} \end{cases} \tag{26}$$

Corrective Maintenance (CM) events are linked to the critical failure event modelling described in Section 2.7.3. The total cost associated with the specific critical failure is calculated as the sum of direct (C_{DIR}) and indirect costs (C_{IND}), as shown in Eq. (27):

$$C_{CM}(t) = C_{DIR}(t) + C_{IND}(t) \tag{27}$$

C_{DIR} represents the cost required for offshore repairs. In the SD model, it is incurred whenever a critical failure is repaired. As different failure modes are considered in this study, the cost is specified by the index (m), as given in Eq. (28):

$$C_{DIR}(t) = \begin{cases} C_{DIR,m} & \text{if the repair of failure mode } m \text{ is completed at } t \\ 0 & \text{otherwise} \end{cases} \tag{28}$$

Both the system preventive maintenance cost ($C_{PM,system}$) and specific corrective maintenance cost ($C_{DIR,m}$) are calculated using a generalized maintenance activity cost ($C_{activity}$) function. This function includes the

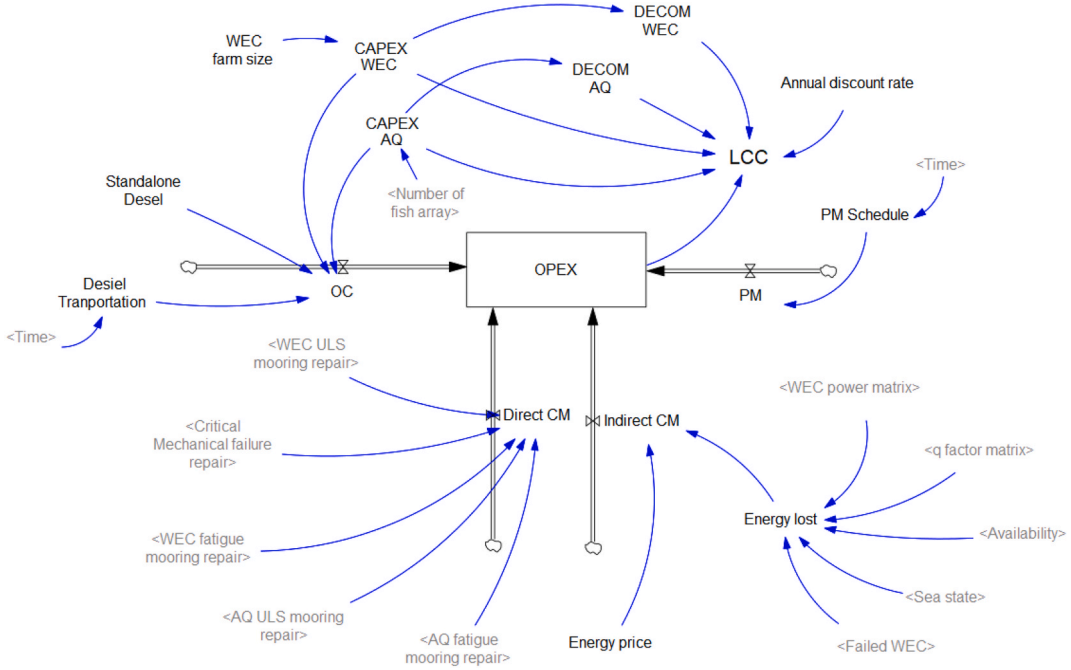

Fig. 7. Developed SD model for Life Cycle Cost (LCC) of the MPOP.

vessel hire cost (C_{vessel}), fuel costs (C_{fuel}), technician costs (C_{tech}), and material costs (C_{mat}), as given in Eq. (29):

$$C_{activity} = C_{vessel} + C_{fuel} + C_{tech} + C_{mat} \tag{29}$$

The detailed relationships for each of the cost components are provided in Eq.(30)–(32):

$$C_{vessel} = C_{mob} + R_{vessel} \cdot \left[\frac{2D_{port}}{V_{vessel}} + T_{activity}\right] \tag{30}$$

$$C_{fuel} = P_{fuel} \cdot F_{rate} \cdot \frac{2D_{port}}{V_{vessel}} \tag{31}$$

$$C_{tech} = N_{tech} \cdot C_{tech} \cdot \left[\frac{2D_{port}}{V_{vessel}} + T_{activity}\right] \tag{32}$$

Where D_{port} represents the distance from main port to the offshore deployment site. V_{vessel} is the vessel speed. $T_{avtivity}$ is the time required for the maintenance activity. R_{vessel} denotes the vessel daily hire rates, and C_{mob} is the vessel mobilisation fee. F_{rate} is the vessel fuel consumption rate, and P_{fuel} is the fuel price. C_{tech} denotes the technician daily rate. N_{tech} represents the number of technicians required for the activity. In practice, these parameters are adopted to reflect the specific requirements of different maintenance activities. For example, routine PM activities require a small Crew Transfer Vessel (CTV) with limited personnel working for a relatively short period. Conversely, critical system failure repair may need to employ a multi-functional workboat and extended repair windows with more experienced technicians (Kamidelivand et al., 2024).

Finally, the indirect CM cost (C_{IND}) represents the financial loss due to the system downtime. It contributes to the C_{OPEX} stock whenever a WEC is in the failed state, as represented in Eq. (33):

$$C_{IND}(t) = \begin{cases} P_{WEC.failed}(t) \cdot P_{electricity} & \text{if there is WEC under downtime} \\ 0 & \text{if all WECs are in operational state} \end{cases} \tag{33}$$

Where $P_{WEC.failed}(t)$ is the potential power output that the failed WEC would have generated at time t, and $P_{electricity}$ is the real-time renewable energy price.

3. Methodology application: A case study of south-east Tasmania

3.1. Scenario description

To illustrate the application of the developed framework, a case study is conducted on a co-located WEC and aquaculture facility in south-east Tasmania, Australia involving quantitative analysis of the MPOP's operational performance.

The southeastern coast of Tasmania has been highlighted for offshore salmon aquaculture, given its optimal environmental conditions and

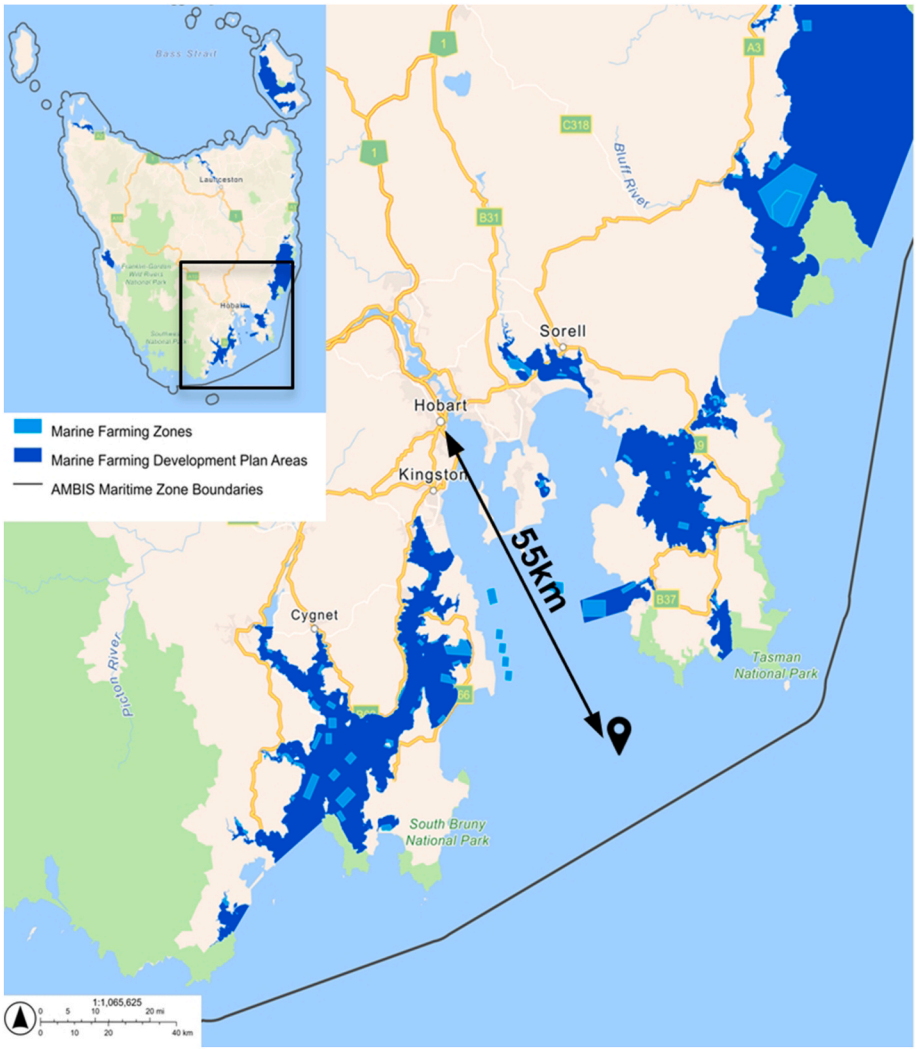

Fig. 8. Selected location for MPOP operation.

proximity to existing aquaculture infrastructure (Lacharite et al., 2021). The existing marine farming zones and development plan areas are mapped and coloured in Fig. 8. As reported by Liu et al. (Liu et al., 2023), Tasmania has been identified as a region with abundant wave energy potential. The area demonstrated in Fig. 8 has a wave energy flux of about 60-80 kW/m due to its advantageous geographical location, providing significant opportunities for wave energy harvesting.

Based on these insights, the Tasmanian MPOP deployment site is selected at the location marked in Fig. 8. General information about this site is summarised in Table 1. The chosen location is situated away from existing coastal aquaculture zones in a more exposed sea area to enable better scalability and more available wave power. This site offers great offshore aquaculture expansion opportunities, feasibility of renewable and off-grid operations. However, due to the increased loads, risks of structural integrity damages under realistic open-ocean conditions require an investigation of the performance of the MPOP in such an environment.

3.2. MPOP system design

An Arrow-configuration CETO 6 WEC farm is considered for powering and protecting a salmon farm. A plausible MPOP layout is configured with eight groups of salmon cages, each with dimensions of 200 m in width (W) and 300 m in length (L). These dimensions are commonly adopted in offshore salmon farm design (Faltinsen and Shen, 2018). To determine the number and layout of the WEC array, several WEC spacings were tested to evaluate the characteristics of the resulting shadowed area. A WEC farm with nine WECs was selected with a spacing between WEC devices of $S = 4\ D$, where D is the diameter of the WEC buoy. This configuration ensures that the attenuated wave field produced by the WEC farm effectively covers the aquaculture facility sitting area. The developed co-located MPOP layout is demonstrated in Fig. 9.

3.3. Environmental modelling

Wave time-series data at the selected location, collected from the Australian Wave Energy Atlas (Hemer et al., 2017), are used to determine the wave height-period joint distribution, presented in Fig. 10a. Representative sea states are identified by clustering, as shown by the markers in the joint distribution plot. The wave direction distribution is shown by a wave rose diagram (see Fig. 10b), which highlights that the predominant wave direction at the site is southwest (SW). This information provides critical insight for selecting the optimal orientation of the WEC farm, such that the layout arrow should point toward the SW, maximising the wave energy capture and downstream shielding.

Detailed sea state parameters, including significant wave height (H_s), peak wave period (T_p), wave directions, and their corresponding occurrence probabilities, are summarised in Table 2. In this paper, it is assumed that wave conditions and wave directions are statistically independent. Numerical simulations are carried out for a total of 64 discrete sea states to represent all combinations of sea conditions and to thoroughly consider the uncertainty with environmental conditions.

3.4. WEC near-field hydrodynamic analysis

Hydrodynamic simulations of a single CETO 6 device, conducted in Orcaflex, produced the power matrix and structural responses used in subsequent analyses. The numerical modelling and installation configuration, including device dimensions, hydrodynamic parameters, and mooring setups, were established based on the proposed approaches by Bao et al. (2024a). Fig. 11 illustrates an overview of device dimensions and installation settings.

Table 1
Potential site information.

Parameter	Value
Coordinates	147.64 ° E, 43.33° S
Distance to main port (Hobart)	55 km
Averaged water depth	50 m

As discussed in Section 2.2.4, the power matrix for the CETO 6 Wave Energy Converter operating at 2 m submerged depth was obtained through numerical simulations at each districted sea state. To capture the responses of the structure in operational conditions, a power matrix is constructed by analysing sea states with $H_s = 0$ - 7 m and $T_p = 3$ - 15 s.

The results presented in Table 3 indicate that CETO 6 demonstrates superior power production capability across a wide range of wave periods. This performance is attributable to its configuration, which enables power capture across all six degrees of freedom, enabling resonant responses to multiple excitation types (e.g., heave, sway, and pitch). However, this flexibility in motion response introduces dynamic instability in severe sea-states. Simulation results show that when significant wave heights exceed 6 m, the device experiences unstable motion. Specifically, the large surge and heave response leads to yaw instability of the WEC device, which results in intermittent tether slackening. This instability mechanism has been experimentally validated in previous studies (Orszaghova et al., 2018). This suggests that deployment at greater submergence depths may be necessary to ensure operational safety and maintain continuous power production under extreme conditions.

3.5. WEC farm power production

By integrating the power matrix into the SNL-SWAN model, a comprehensive wave propagation analysis of the WEC farm is conducted. The results demonstrate that in-farm interactions between individual WEC devices can substantially reduce the total power output, with the magnitude of the reduction heavily dependent on deviations in the incident wave direction.

Fig. 12 demonstrates the distribution of k_d within the WEC farm using contour plots, clearly illustrating blocking effects among individual devices. Darker regions indicate lower k_d values and a reduction in significant wave height. When waves approach from the predominant southwest direction, (aligned with the array arrowhead, from left to right in Fig. 12a), the array operates at peak efficiency. WECs generate approximately 216 to 219 kW, indicating a balanced distribution of absorbed wave energy throughout the farm with minimal interaction. In contrast, when waves approach from the west (from left to right in Fig. 12b), significant blocking effects are observed. Upstream WEC units (WECs 1, 2, 4, 6, and 8) absorb substantial incoming wave energy, leaving considerably reduced wave energy for downstream units. Consequently, downstream devices show notable reductions in power output: WECs 3, 5, 7, and 9 produce approximately 64.8 kW, 51.2 kW, 34.4 kW, and 31.1 kW, which are significantly below their rated power and generation potential.

To accurately quantify array power production, the q-factor was derived from simulation results for each sea state. The q-factor matrix, presented in Table 4, explicitly characterises the WEC farm efficiency under combinations of wave conditions and incident directions. The sea-state indicators are derived from the numbering in Table 2. For instance, the indicator “SW-2" corresponds to waves coming from the southwest direction with the wave conditions of Sea-state 2, where $H_s = 1.6$ m and $T_p = 9$ s.

3.6. WEC farm wave shadowing effects

In addition to the in-farm interactions, the wave propagation modelling enables a comprehensive assessment of the shadowing effects downstream WEC array. Given the predominant wave direction from the southwest, the analysis focuses on wave height reduction patterns for waves from this direction. Fig. 13 illustrates the spatial distribution of the k_d value downstream of the WEC farm. Wave height reduction is

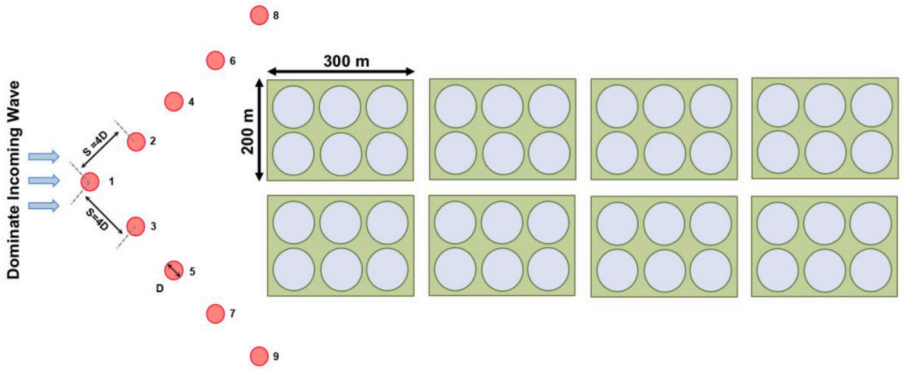

Fig. 9. The adopted design of MPOP.

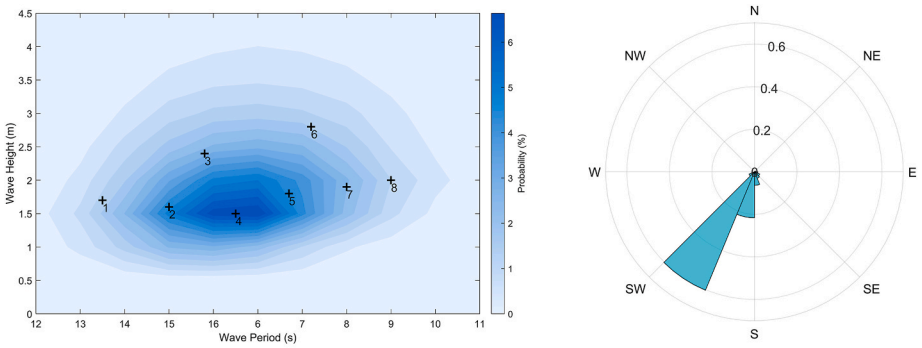

Fig. 10. a) Wave height-period joint distribution, and b) wave rose diagram of the selected deployment site.

Table 2
The environmental conditions at the case study site, including wave conditions, wave directions and their occurrence probabilities.

Sea state number	H_s (m)	T_p (s)	Probability	Wave direction	Probability
1	1.7	7.5	0.0600	N	0.0006
2	1.6	9.0	0.1900	NE	0.0020
3	2.4	9.8	0.1100	E	0.0187
4	1.5	10.5	0.2100	SE	0.0530
5	1.8	11.7	0.2000	S	0.1778
6	2.8	12.2	0.0600	SW	0.7425
7	1.9	13.0	0.1200	W	0.0047
8	2.0	14.0	0.0500	NW	0.0007

most pronounced immediately downstream of the WEC farm, and the shadowing effect gradually diminishes with distance. Beyond approximately 2 km downstream, the effect is weakened significantly, such that wave height variability is increased.

To quantify the uncertainty in wave height reduction within the aquaculture area, k_d values are obtained for each section of the area. For aquaculture module (illustrated as numbered black boxes in Fig. 13), data points were extracted from the numerical grid at a resolution of 1 m, resulting 60000 simple points per cage group. Due to the symmetrical MPOP layout about the central horizontal axis, wave height reduction data (k_d) is assessed only for the four upper modules of the salmon farm (modules 1-4), with the flow conditions assumed to be identical in the lower counterparts. This will determine how the shadowing effectiveness changes spatially. As shown in Fig. 14a, the mean value of k_d increases progressively with distance, confirming a weakening wave height reduction effect further downstream.

It is also observed that variability in k_d is higher at location closest to and furthest from the WEC farm, as shown in the boxplots in Fig. 14a. The large fluctuations in these modules most likely arise from complex local hydrodynamics and undeveloped flow. Such fluctuations in the wave condition add to design and operational uncertainties, where varying loads may increase the risks associated with structural resonance, fatigue damage, and unstable operating conditions for aquaculture facilities, with potential impacts on fish welfare and growth. These results emphasise the importance of optimally positioning aquaculture systems relative to the WEC farm to balance wave protection, minimise hydrodynamic uncertainty, and maintain stable aquaculture operations.

3.7. Aquaculture farm hydrodynamic analysis

3.7.1. Salmon farm structure numerical modelling

The salmon cage modelled in this study has 50 m diameter, featuring a 15 m high cylindrical section and a 10 m high conical bottom. The floating collar, constructed from High-density Polyethylene (HDPE) pipes, provides the necessary buoyancy to maintain cage volume, while the sinker tube and bottom central mass provide tension to ensure net shape stability. Detailed dimensions and structural properties of the employed salmon cage design, adopted from previous validated studies (Shen et al., 2018; Nasyrlayev et al., 2023), are listed in Table 5.

A grid mooring system is used for station keeping of the salmon farm due to its space efficiency, structural redundancy, and reliable load distribution capabilities (Tang et al., 2020). The mooring structure comprises bridle lines, surface buoys, steel coupling plates, frame lines, anchor lines, and anchors. Specifically, the mooring arrangement includes 14 main anchor lines connected to steel coupling plates, with four frame lines encapsulating each cage cell. Each coupling plate is attached to a buoy at the water surface to maintain buoyancy and appropriate pre-tension in the anchor lines. Additionally, cages are connected to these coupling plates via four groups of bridle lines (two bridle lines per group), which effectively constrain horizontal motions of the cages (Li

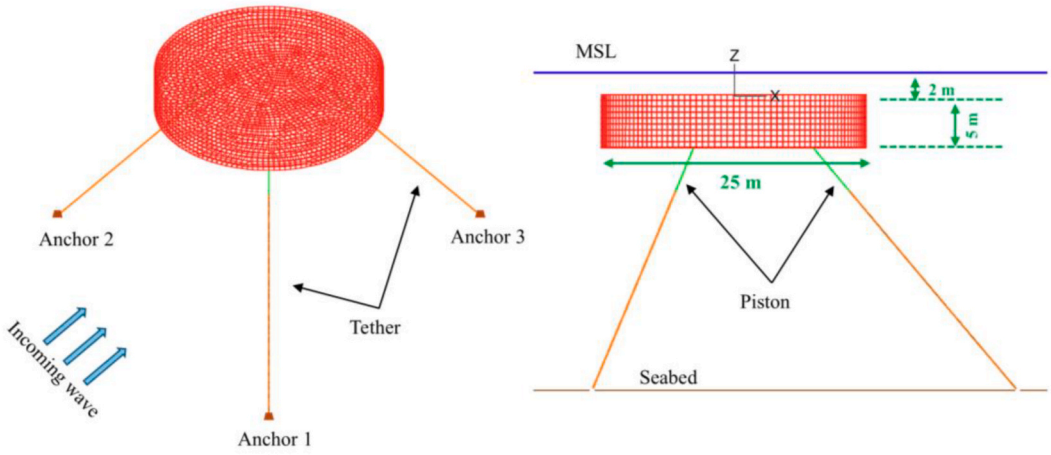

Fig. 11. Developed Orcaflex numerical model of CETO 6 WEC.

Table 3
Power matrix (kW) of CETO 6 WEC.

$H_s(m)$	$T_z(s)$												
	3	4	5	6	7	8	9	10	11	12	13	14	15
1	59	155	166	211	290	361	189	394	501	493	467	428	387
2	-	328	376	473	588	598	416	601	791	855	944	856	767
3	-	-	682	842	884	896	701	1203	1125	1237	1091	1290	1130
4	-	-	-	1080	1341	1385	1176	1500	1500	1402	1500	1402	1373
5	-	-	-	1500	1500	1500	1500	1500	1500	1500	1500	1500	1500
6	-	-	-	-	-	-	-	-	-	-	-	-	-
7	-	-	-	-	-	-	-	-	-	-	-	-	-

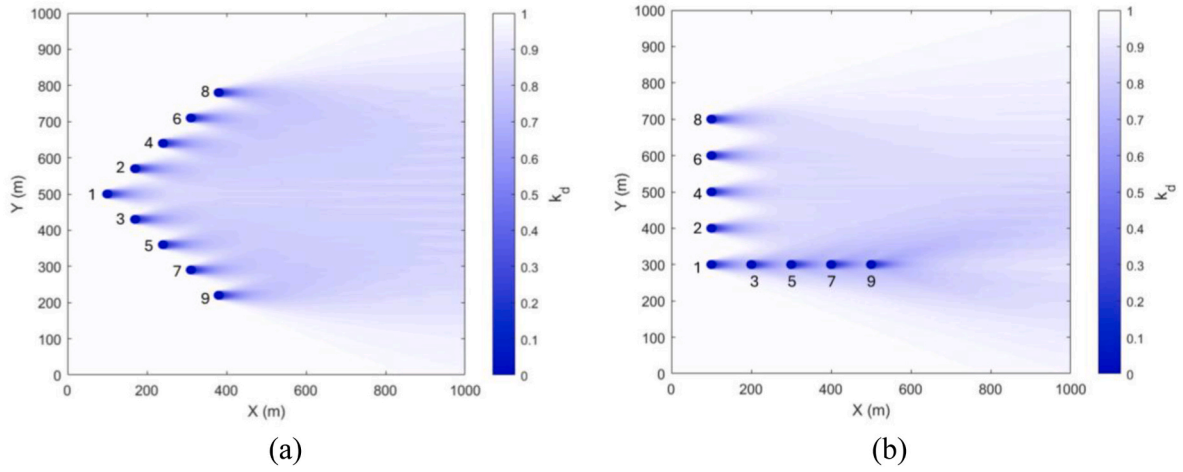

Fig. 12. The wave disturbance coefficient contour plots propagating through the WEC farm with different incoming wave direction a) Southwest wave direction and b) West wave direction.

et al., 2020).

As demonstrated in Fig. 15, the numerical model of the salmon cage array is modelled with 8 and 4 trusses arranged horizontally in the cylindrical and conical sections of the cage, and 16 trusses placed vertically. The floating collar and sinker tube components are modelled in OrcaFlex explicitly as homogeneous pipes to obtain bending stiffness, buoyancy, and weight characteristics. For other mooring system components without specific parameter definitions, default values are employed from the Orcaflex built-in *line type wizard* database.

3.7.2. Aquaculture farm mooring tension

To further assess the protective advantages of co-location, specifically in terms of the aquaculture mooring integrity, the distribution of k_d within the entire operational area of the aquaculture farm (dashed blue box in Fig. 13) is demonstrated using the boxplot (Fig. 14b). The results indicate that the WEC farm reduces incoming wave height by 8%-23% within the downstream area. Five k_d values are then selected from the distribution, including the minimum, first quartile, median, third quartile, and maximum, to scale incident wave heights across all eight sea states. This resulted in 40 cases for simulating the aquaculture array operating within the shadowed zone. A current velocity of 0.25 m/s is

Table 4
Input q-factor matrix in SD.

Sate-state indictors	q-factor	Sate-state indictors	q-factor	Sate-state indictors	q-factor	Sate-state indictors	q-factor
N-1	0.6697	E−1	0.6697	S-1	0.6489	W-1	0.7489
N-2	0.6686	E−2	0.6686	S-2	0.6408	W-2	0.6408
N-3	0.6889	E−3	0.6889	S-3	0.6876	W-3	0.6876
N-4	0.6637	E−4	0.6637	S-4	0.6354	W-4	0.6354
N-5	0.6864	E−5	0.6864	S-5	0.6639	W-5	0.6639
N-6	0.6894	E−6	0.6894	S-6	0.6880	W-6	0.6880
N-7	0.6894	E−7	0.6864	S-7	0.6856	W-7	0.6856
N-8	0.6866	E−8	0.6866	S-8	0.6858	W-8	0.6858
NE-1	0.9893	SE-1	0.6904	SW-1	0.9892	NW-1	0.6904
NE-2	0.9893	SE-2	0.6682	SW-2	0.9893	NW-2	0.6682
NE-3	0.9896	SE-3	0.7340	SW-3	0.9896	NW-3	0.7340
NE-4	0.9893	SE-4	0.6494	SW-4	0.9893	NW-4	0.6494
NE-5	0.9893	SE-5	0.7218	SW-5	0.9893	NW-5	0.7218
NE-6	0.9898	SE-6	0.7345	SW-6	0.9898	NW-6	0.7345
NE-7	0.9893	SE-7	0.7304	SW-7	0.9893	NW-7	0.7304
NE-8	0.9894	SE-8	0.7307	SW-8	0.9894	NW-8	0.7307

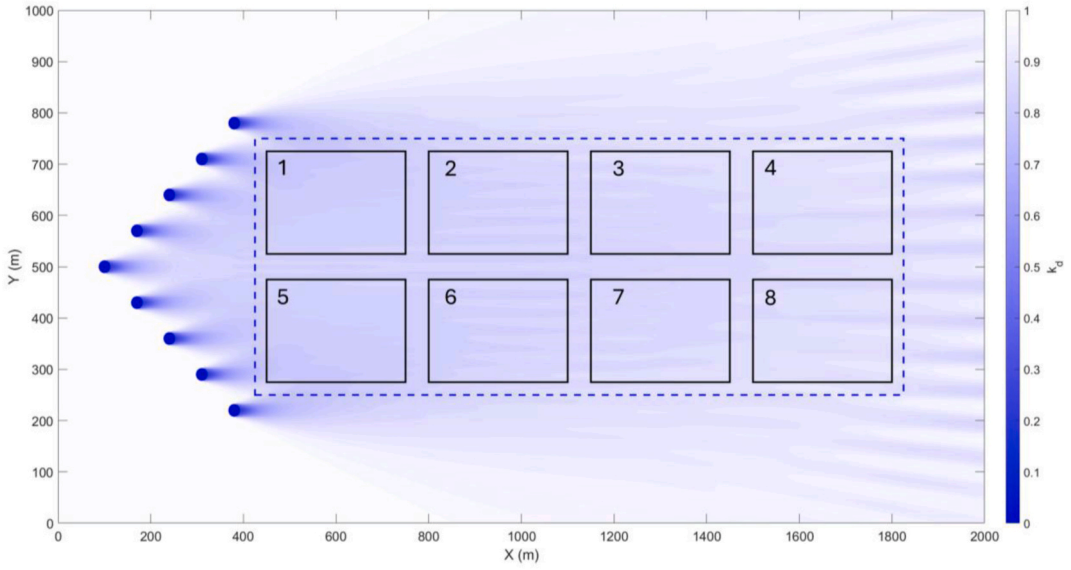

Fig. 13. WEC farm shadowing area and aquaculture array layout. The numbered boxes represent individual aquaculture cage arrays.

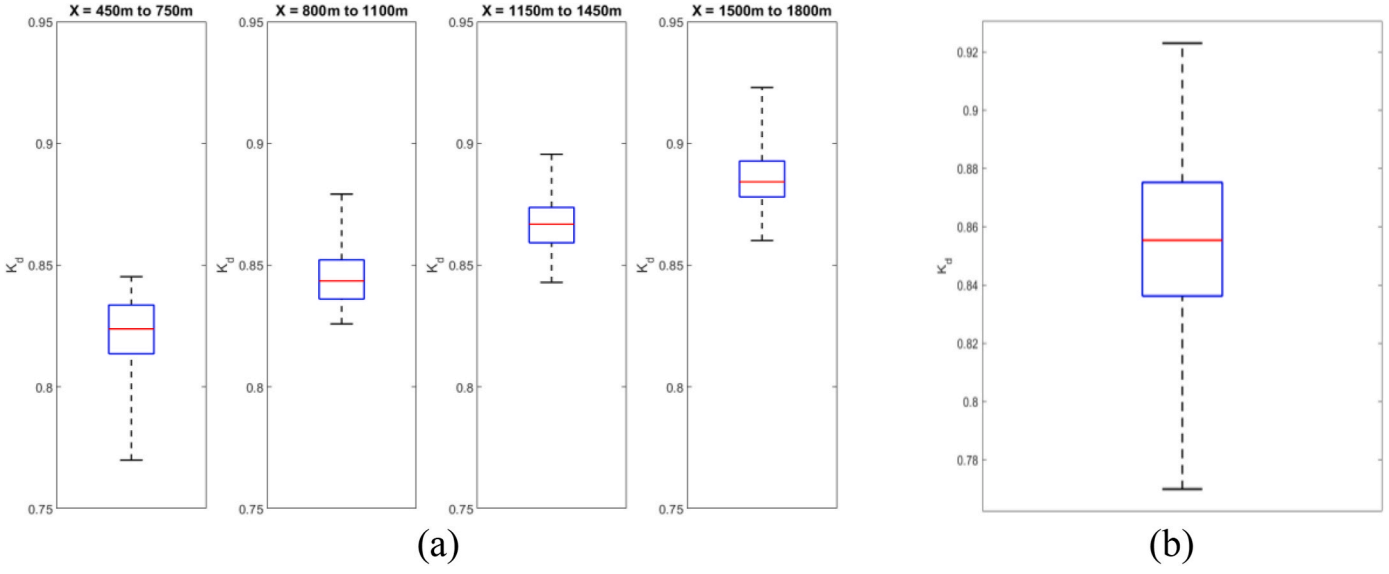

Fig. 14. The distribution of disturbance coefficient within the WEC shadow zone a) variation of k_d values with increasing horizontal distance downstream the WEC array; b) the overall distribution of k_d values across the entire aquaculture farm area.

Table 5
Specifications of the gravity-based fish cages used in case study.

Component	Parameter	Value	Unit
Net cage	Diameter	50	m
	Vertical net height	15	m
	Cone net height	10	m
	Net twine diameter	3.25	mm
	Net twine length	14.3	mm
	Net solidity	0.26	-
	Net twine density	1125	kg/m^3
	Center point mass	200	kg
Floating collar	Collar outer diameter	50	m
	Cross-sectional diameter	0.45	m
	Wall thickness	55	mm
	Collar mass per unit length	64.8	kg/m
	Bending stiffness	1465.47	kNm^3
Sinker tube	Tube diameter	51.8	m
	Submerged mass per unit length	50	kg/m
	Submerged depth	17	m
	Bending stiffness	200	kNm^2
Buoys	Number of buoys	12	-
	Diameter	1.55	m
	Height	2.34	m
	Chain length	7	m
	Coupling plate mass	55	kg
Bridle lines	Material	Polyester	-
	Length	49.22	m
	Diameter	22.4	mm
Frame lines	Material	Nylon	-
	Length	100	m
	Diameter	51.2	mm
Mooring lines	Material	Nylon	-
	Length	112.5	m
	Diameter	51.2	mm

also applied according to the environmental modelling at the implementation site (BOM). Tension in the aquaculture anchors is quantified under a realistic, spatially variable wave shadowing zone.

Simulation results for anchor line tensions under a representative sea state with $H_s = 1.8$ m and $T_p = 11.7$ s are shown in Fig. 16a. Three anchor lines 2, 3, and 4 (see layout in Fig. 15) at the front of the aquaculture farm facing the incoming waves are analysed due to direct exposure to wave loads. Tensions increased gradually from an initial transient phase (approximately 0–200 s) to a steady-state phase as the aquaculture farm transitioned from static equilibrium to dynamic equilibrium under combined wave and current forcing. The steady-state phase, representing operational conditions, is the focus for reliability assessment and thus, being used for further analysis.

As shown in Fig. 16a, the time-series tension in anchor lines 2 and 4 are almost identical, reflecting the symmetric layout of the aquaculture mooring system and alignment of the incoming wave direction with the aquaculture array orientation. Notably, anchor line 3 shows significantly higher values with larger fluctuations, identifying itself as the critical component for potential ULS and fatigue failures.

A comparison of anchor line 3 tensions between un-protected and protected scenarios using the mean k_d value of 0.855 is plotted in Fig. 17b. A clear reduction in anchor line tension is observed when the aquaculture system is protected with the WEC array, while the fluctuation pattern remains consistent with the un-protected scenario due to the unchanged wave period.

Further analysis of the influence of uncertainty k_d on aquaculture anchor tensions uses corresponding R_{tr} values derived from numerical simulations of the aquaculture array. The relationship between the conducted k_d distribution and the resulting R_{tr} range is presented in Fig. 17a. The result indicates a clear positive correlation: lower the k_d value (stronger shadowing) corresponds to lower the resultant R_{tr}, indicating greater reduction in mooring tension. However, the results also reveal that stronger wave height reduction scenarios exhibit greater variability and uncertainty in the R_{tr}, as indicated by wider boxplot ranges in Fig. 17a.

The distribution of R_{tr} across the shadowed aquaculture area is then collected and fitted with a Weibull distribution, as shown in Fig. 17b, yielding a shape parameter of 32.12 and a scale parameter of 0.94. This statistical fit provides a quantitative basis for incorporating wave-shadowing uncertainty into the MPOP performance SD model. In the SD model, R_{tr} is randomly sampled from its probability distribution to scale the mooring tension of the aquaculture farm for protected conditions. The protection effect, in turn, influences the occurrence of mooring critical failure.

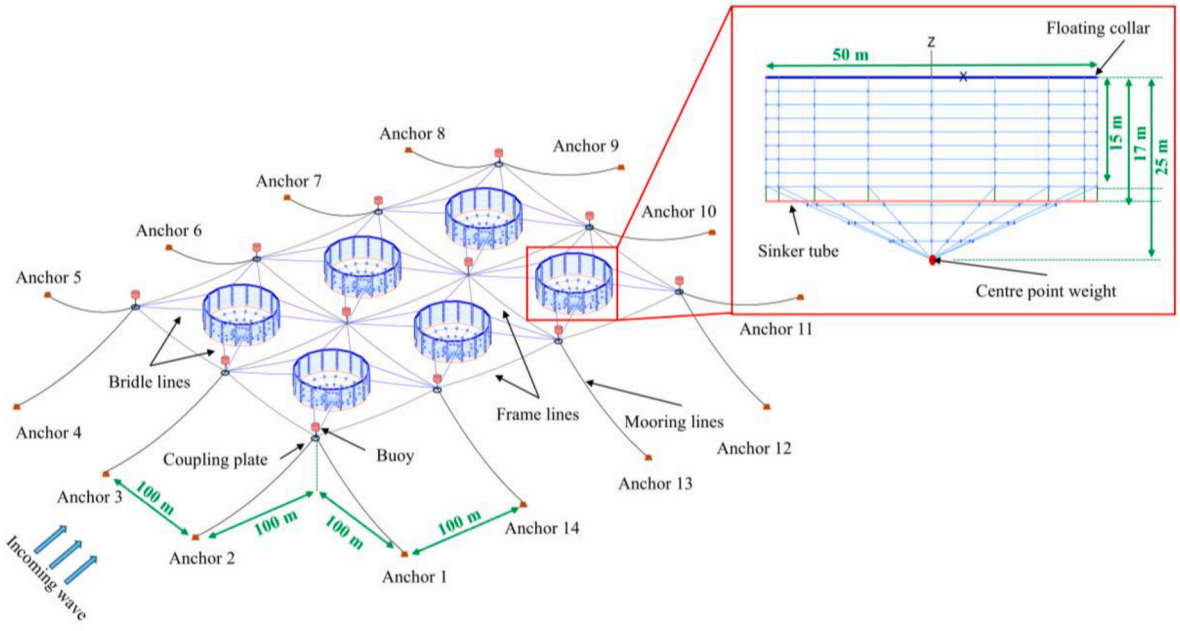

Fig. 15. Employed numerical model of the aquaculture cage array.

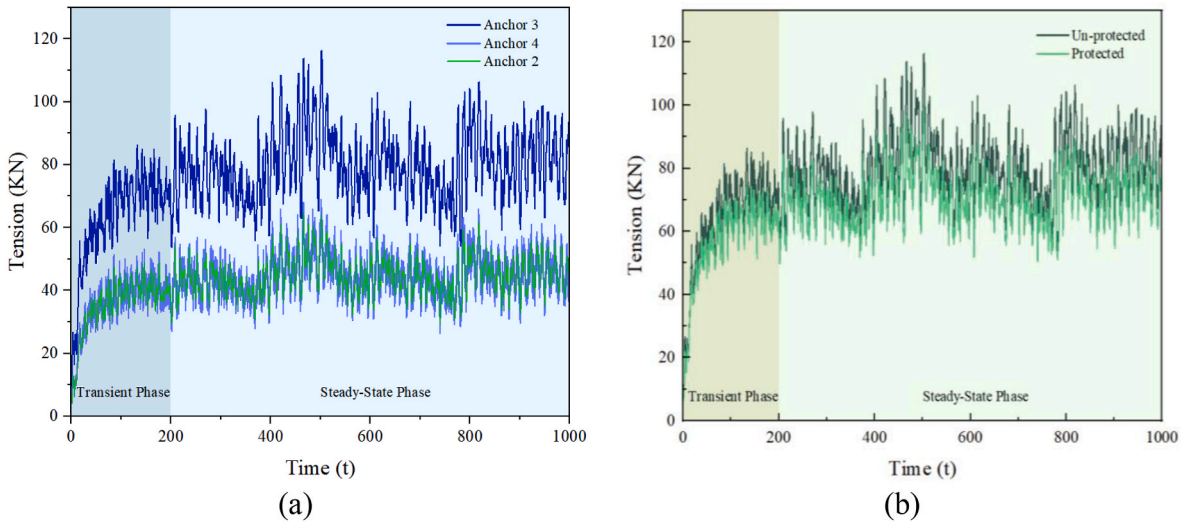

Fig. 16. Simulation results of aquaculture cage array anchor line tension under sea state ($H_s = 1.8$ m and, $T_p = 11.7$ s): a) anchor lines 2-4 (see Fig. 15) without WEC protection, and b) comparison of anchor line 3 under un-protected and protected conditions ($k_d = 0.855$).

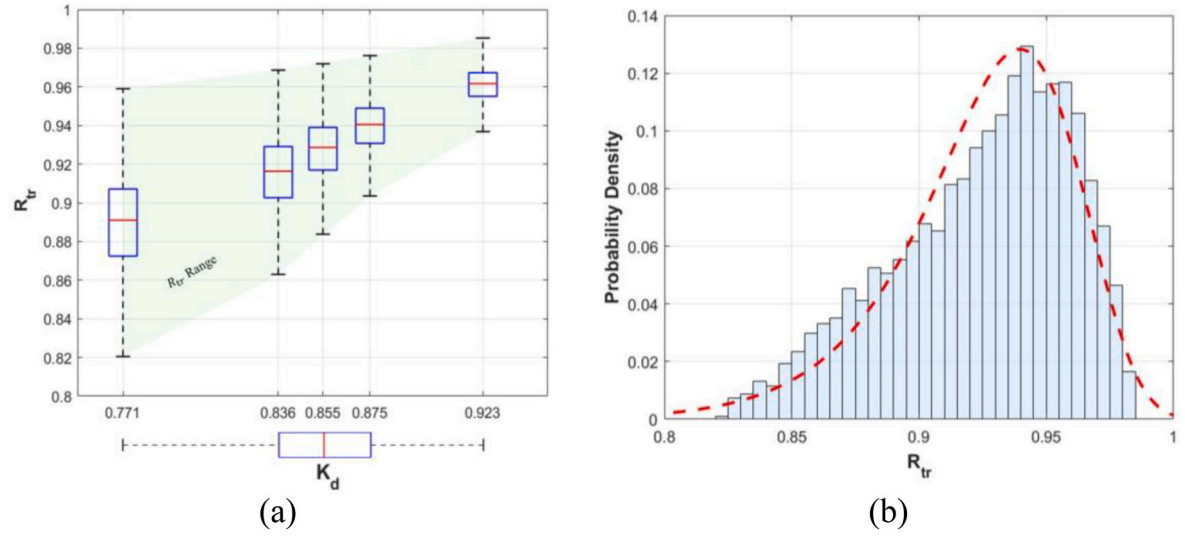

Fig. 17. Results of the uncertainty quantification of the WEC farm protection effects highlighted by a) tension reduction factor values R_{tr} for the aquaculture array mooring lines, and b) fitted Weibull distribution to the obtained R_{tr} values.

3.8. System dynamic modelling

3.8.1. Aquaculture farm food production

Atlantic salmon is selected as the aquaculture species in this study due to Tasmania's well-established salmon farming practices and substantial market potential for seafood supply. The Atlantic salmon farming cycle spans approximately 24–40 months, with key growth stages predominantly occurring in seawater. Initially, fertilised eggs are hatched into juvenile salmon, which are raised in controlled freshwater systems on land until they reach a weight of approximately 100 -150 g. During smoltification, these juveniles gradually adapt to seawater conditions and are transferred to offshore farms. In this phase, these juveniles become smolts and grow from 100 to 1000 g. Then, in offshore cages, the salmon smolts enter an accelerated growth stage, gaining weight from approximately 100 g to a market size of around 4.5 - 5.5 kg. They are then harvested and transported to land for slaughter and further processing (Stead and Laird, 2002).

This study specifically models a 24-month offshore farming cycle consisting of three distinct stages: a 10-month smoltification stage, a 10-month accelerated growth stage, and a final 4-month period consisting of harvesting and relaxing, during which the farm is emptied and prepared for the next farming cycle. The employed salmon growth and mortality rates, which vary depending on the farming stage, are summarised in Table 6 (Bujas et al., 2022). During the simulation of each farming stage, corresponding growth rates are sampled randomly from a normal distribution, characterised by a mean growth rate of 0.09

Table 6
Atlantic salmon growth stage characteristic parameters.

Farming stage	Time	Growth rate range	Mortality rate range	Harvest rate	Unit
Smoltification	1st-10th month	0.08-0.10	0.016-0.020	-	Kg/ month/ fish
Accelerated growth	10-20 month	0.35-0.45	0.053-0.068	-	Kg/ month/ fish
Harvesting	20-24 month	-	-	$2S_{fish}$	Kg/ month

kg/month/fish for the smoltification stage and 0.4 kg/month/fish for the accelerated growth stage, each with a standard deviation of 0.01. Salmon mortality rates are adopted based on industry data from MOWI (MOWI, 2020), which reports a mortality rate of 20% of the growth rate during smoltification and 15% during the accelerated growth stage, reflecting slightly higher vulnerability of salmon juvenile. Harvesting is conducted over a two-week period at the end of the accelerated growth stage.

3.8.2. Aquaculture farm energy demand

The energy needed to support the offshore aquaculture operations varies significantly across different salmon farming stages, mainly because of the changing feeding system workloads. Given the limited availability of time-based energy consumption data from Australian offshore aquaculture systems, this paper adapts validated energy usage profiles from the Norwegian aquaculture industry. To ensure accuracy and relevance of this energy consumption profile for the Australian offshore salmon farming context, adjustments are made to account for significant differences in operational practices between Norway and Australia. Baseline data is collected from the Teistholmen salmon farm, which comprises six 50 m-diameter open offshore net cages, consistent with the array configuration selected for this case study. Norwegian data indicate that energy consumption peaks during feeding hours between 7 a.m. and 4 p.m. Energy consumption in the smoltification stage is assumed to be approximately 25% lower than in the accelerated growth stage due to reduced feeding activity. During the harvesting state, only minimal power consumption (around 5 kW) is required for maintaining basic barge operations, as reported by MOWI (MOWI, 2020).

The Ocean Energy System (OES) Offshore Aquaculture Report indicates that Australian salmon farming operations consume approximately seven times more energy compared to equivalent Norwegian farms to produce a similar biomass of salmon (Freeman et al., 2022). Hemer et al. (Hemer et al., 2020) also highlight that the stationary energy demands of offshore aquaculture facilities, excluding ventilation and vessel transportation, account for approximately 34% of the total energy consumption in Australian salmon farming. To realistically represent the higher energy demands characteristic of Australian offshore aquaculture, a scaling factor of 2.38 (7×0.34) is applied to the baseline profile. Fig. 18 presents the adjusted hourly energy consumption profile used in the SD Model.

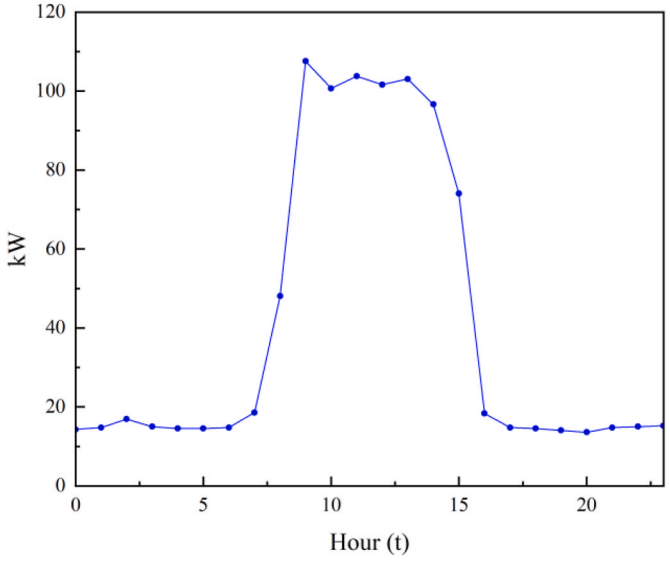

Fig. 18. Daily power consumption profile of the selected aquaculture system in the Australian environment. The profile is derived from Norwegian aquaculture energy consumption data and scaled by a factor of 2.38 to represent the higher operational energy demand of Australian offshore salmon farming.

3.8.3. MPOP availability and failures

Table 7 summarises key WEC subsystems and components, their potential failure modes, failure rates, and severity classifications, which are mostly adopted from previous research (Kamidelivand et al., 2024; Göteman et al., 2018; Rhinefrank, 2016).

The system annual failure rate is obtained for each severity by summing all component failure rates with the same severity. Critical failure of the mooring system for both WEC and aquaculture structures is dynamically simulated under various sea states, as introduced in Section 2.7.3.

3.8.4. MPOP life-cycle cost

Due to the limited availability of detailed cost data, particularly for Australian offshore aquaculture and WEC farm developments, established cost parameters from the European offshore industries have been carefully adopted and converted to Australian dollars (AUD) to ensure accuracy and relevance. Detailed capital expenditure (CAPEX) and decommissioning cost components of the MPOP project are summarised in Table 8 (Têtu and Fernandez, 2020). Additionally, C_O is assumed to be 4% of the total CAPEX annually (Têtu and Fernandez, 2020), resulting in an annual expenditure of approximately 4.36 MAUD/year. An 7% Annual discount rate is adopted in this study from the International Energy Agency (Electricity, 2020).

Regarding MPOP maintenance costs, both CM and PM are considered, where PM is performed on a scheduled biennial basis. As a major contributor to maintenance in offshore locations, two vessel types are considered in this paper, which are a crew transfer vessel (CTV) for common PM and a multi-functional workboat for CM. The relevant data to maintenance of case study MPOP, including vessel details, labour requirements, duration, and material costs, are provided clearly in Table 9 (Kamidelivand et al., 2024; Kumar et al., 2024). While the vessel

Table 7
CETO 6 WEC components and failure data used for availability assessment. mf: minor failure, Mf: major failure, Cf: critical failure.

Subsystem	Components	Failure modes	Annual failure rate	Severity
Structure	Buoy	Minor material loss	0.300	mf
		Deformation & dents	0.030	Mf
		Hull severe crack	0.010	Cf
PTO	Belt	Surface damage	0.104	mf
		Fracture/ Separation	0.052	Mf
	Pully system	Surface damage	0.660	mf
		Fracture/ Separation	0.023	Mf
	PTO hull	Crack/Leakage	0.010	mf
	Damper	Crack	0.030	mf
	Belt & mooring connection	Fracture/ Separation	0.020	Cf
	In-Buoy energy conversion unit	Structural failure	0.018	Mf
Transmission & Control	Frequency converter	Fail to function on demand	0.296	mf
		Low output	0.034	mf
	Switchgear	Fail to function on demand	0.010	mf
	Sensor & Controller	Signal failure	0.130	Mf
		Fail to function on demand	0.037	mf
		Minor in-service problem	0.099	mf
Mooring	Joint	Fracture/ Separation	0.030	Mf
	Anchor	Material loss	0.030	Mf
	Mooring tendon	Surface damage	0.603	mf
		Line break	Sea-state dependent	Cf

Table 8
Capital and decommissioning cost parameters for the MPOP system.

Cost Category	Description	Value	Unit
CAPEX	Single WEC	10.8	MAUD
	Single aquaculture array	1.5	MAUD
	License	1	MAUD
	System power connection	1.8	MAUD
DECOM	WEC farm	14.6	MAUD
	Aquaculture farm	1.2	MAUD

Table 9
Preventive and corrective maintenance cost parameters for MPOP system.

Cost Category	Description	Value	Unit
PM Vessel	Fuel consumption	150	L/h
	Mobilization fee	0.014	MAUD
	Daily hire rate	0.01	MAUD
	Speed	12	Knots
MPOP System PM	Material cost	0.035	MAUD
	Technician daily rate	200	AUD/day
	Number of technicians required	5	-
	PM activity time	2	Days/WEC or cage group
CM Vessel	Fuel consumption	300	L/h
	Mobilization fee	0.044	MAUD
	Daily hire rate	0.035	MAUD
	Speed	17	Knots
WEC system CM	Mooring repair time	25	Days/device
	Mechanical component repair time	20	Days/device
	Mooring material cost	0.1	MAUD
	Mechanical component material cost	0.14	MAUD
	Technician daily rate	300	AUD/day
	Number of technicians required	12	-
AQ farm CM	Mooring replacement time	15	Days
	Mooring material cost	0.18	MAUD
	Technician daily rate	250	AUD/day
	Number of technicians required	8	-

fuel price is adopted as 1.63 AUD/L. Additionally, the renewable energy price of 83 AUD/MWh is adopted in evaluating the down-time energy cost of the WEC farm.

3.9. MPOP system performance analysis

Following the development of the SD model, its capabilities are evaluated by quantifying the synergy effect from co-locating the WEC farm and aquaculture system. Several carefully defined scenarios are then simulated to assess the MPOP system's performance under varying and uncertain environmental and operational conditions.

3.9.1. Quantify co-location synergy effect

To evaluate the economic and operational advantages of the proposed co-located arrangement, a comparative analysis is undertaken against a stand-alone aquaculture and WEC farm scenario. Unlike the integrated system, a stand-alone aquaculture farm lacks a direct renewable power supply from a co-located WEC farm. Therefore, it is assumed to rely on diesel-powered generators for continuous offshore operation. This configuration introduces initial costs for generator procurement and higher operational costs associated with generator maintenance and diesel fuel transportation. Also, the absence of WEC farm protection increases environmental loads on the aquaculture farm, with potential increases in mooring system failures and CM costs. PM activities for the aquaculture and energy systems also had to be conducted independently, increasing vessel mobilisation and rental costs. Specifically, a 110 kW diesel generator and a supplementary 10 kW backup generator is assumed per aquaculture farm array, with monthly diesel transportation and the associated maintenance activities. The detailed cost components adopted for modelling the stand-alone diesel-powered aquaculture operation are summarised in Table 10.

The SD simulation results for the 20-year project lifespan confirm the operational and economic superiority of the co-located configuration. As illustrated in Fig. 19a, the stand-alone aquaculture farm experiences a significantly higher frequency of critical failures due to the absence of protection from the upstream WEC farm. This directly translates into the increased number of CM activities and associated costs, as demonstrated in Fig. 19b. The stand-alone scenario accumulates a system LCC of 393.4 MAUD. In contrast, the co-located MPOP scenario achieves an LCC of 272.5 MAUD, representing an over 30% cost reduction. This substantial cost saving confirms that the co-locating MPOP is an effective solution for enhancing system reliability and development cost-effectiveness. Therefore, the co-located configuration is adopted as the baseline case in the following sensitive analyses of this paper, which aim to evaluate the performance of the MPOP under uncertainty.

The WEC farm continuously generates surplus energy, in addition to supplying the aquaculture system, at an average rate of 2.6 MW, as demonstrated in Fig. 20a. This is expected to accumulate approximately 4.0E+05 MWh of energy over the project life. This outcome confirms that the WEC array can reliably supply sufficient energy to meet the operational demands of eight aquaculture arrays without requiring external energy sources. The surplus energy will enable system expansion, for reasons such as supporting other offshore activities, powering service vessels, or potentially power provision to the grid.

For the system food production, the aquaculture farm productivity is shown in Fig. 20b over two fish farming cycles. The average production is approximately 3260 tonnes per cage per cycle. This productivity level is substantial and aligns with mature industry benchmarks from the Norwegian salmon farming sector, which reports typical capacities of 3200 tonnes per cage (Syse, 2016).

3.9.2. Operational sensitive analysis

Several scenarios were designed for MPOP system performance analysis to further demonstrate the effectiveness of the developed SD model. These scenarios explore uncertainties associated with operational parameters, such as components failure rate, corrective maintenance duration, and aquaculture power demand, that significantly influence system availability, output, and overall costs. The rationale, scenario definition, and parameterization are listed in detail in Table 11.

S1: Maximum shadowing effects

This simulation is conducted to investigate the potential benefits of achieving maximum protection against wave loads across the entire aquaculture farming area. The scenario is assessed by adopting the minimum observed mooring tension reduction factor ($R_{tr} = 0.82$) into the SD simulation.

Fig. 21 compares system performance under maximum shadowing effects with that of the baseline co-located scenario. The results highlight that maximum wave protection reduces the occurrence of critical

Table 10
Components of the operating costs of stand-alone diesel-powered aquaculture system.

Parameter	Value	Unit
110 kW diesel generator	0.033	MAUD
10 kW diesel generator	0.014	MAUD
Diesel consumption rate	60000	L/year
Diesel transportation cost	0.034	MAUD/month
Generator O&M cost	0.0014	MAUD/year

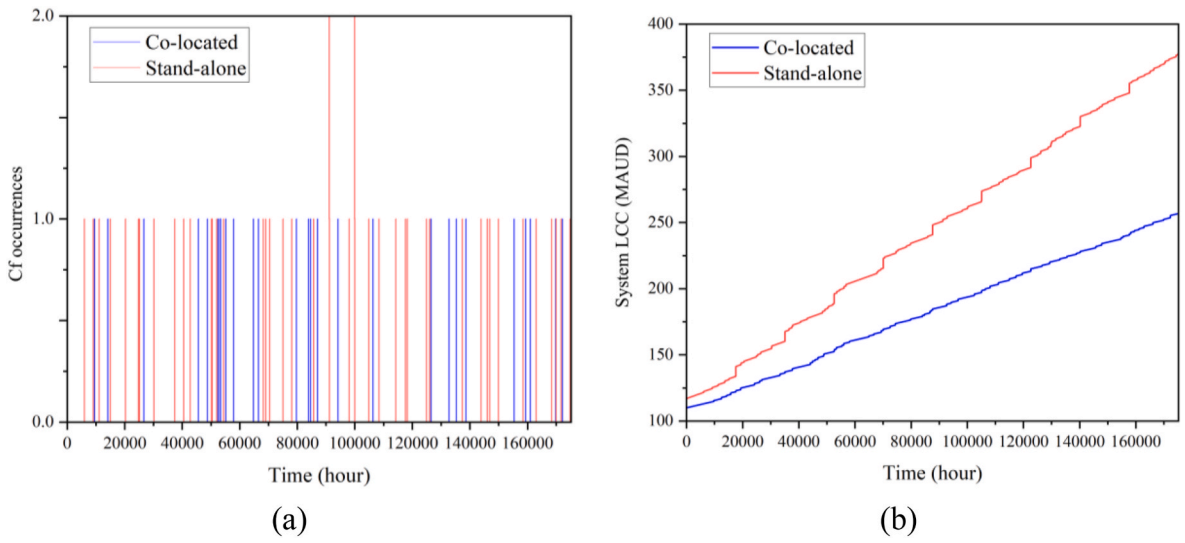

Fig. 19. Comparison of aquaculture system performance between co-located and standalone configurations: a) critical failure events occurrences during a 20-year aquaculture farm life-cycle and b) accumulated life-cycle costs.

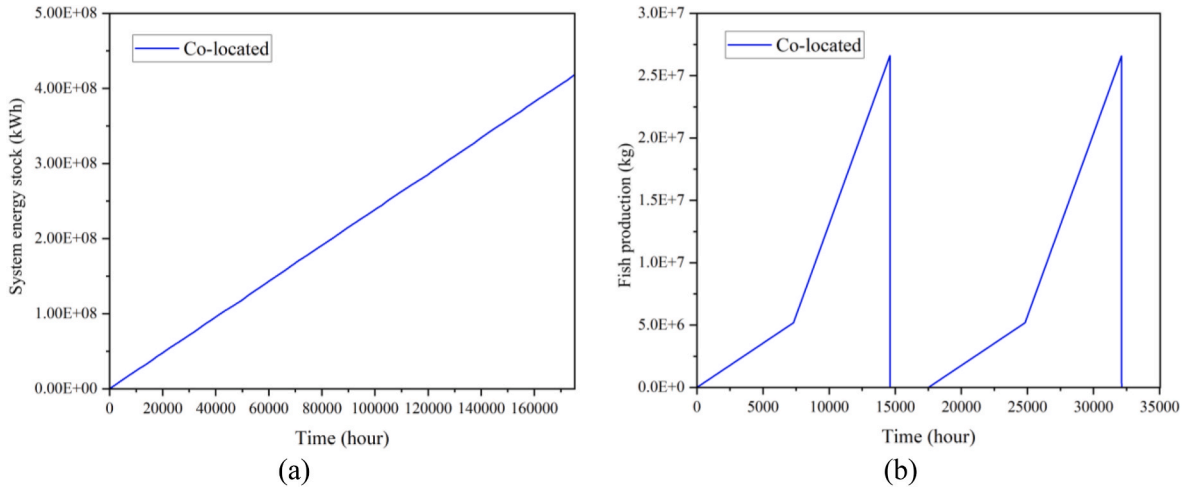

Fig. 20. Baseline scenario system performance under the co-located MPOP configuration: a) accumulated energy production surplus to supplying aquaculture system needs, and b) fish production over two harvesting cycles.

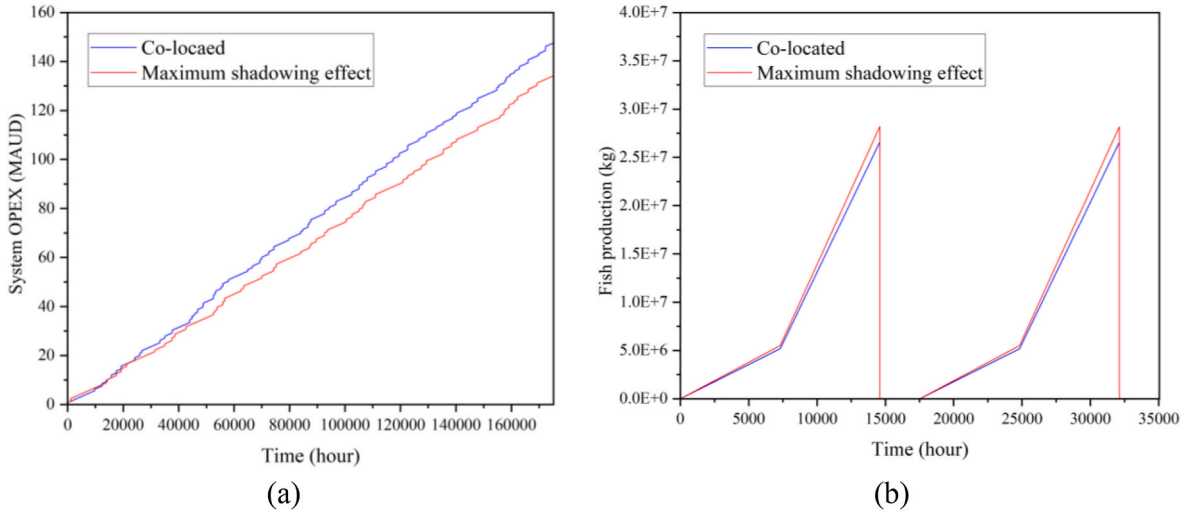

Fig. 21. Comparison between the baseline and maximum shadowing scenarios: a) Accumulated OPEX, and b) Aquaculture fish production.

Table 11
Description of SD simulation scenarios used in the case study.

Indicator	Scenario	Description
S1	Maximum protection effects	Given the inherent uncertainty in protection effects (wave height reduction) resulting from co-location, this scenario examines an idealized condition assuming maximum theoretical protection across the entire aquaculture farming area. This is performed to identify opportunities for optimal performance.
S2	Fluctuating aquaculture system power demand	The energy demand of the aquaculture system may fluctuate due to variable feeding intensities, salmon activity, and environmental conditions. To reflect on this, a ±20% variation in the hourly power demand is introduced into the SD model in this scenario.
S3	WEC system degradation	Over prolonged offshore operations, the WEC devices will naturally degrades due to component wear, structural deterioration, and ageing. To investigate the long-term impact of this degradation on system performance, a time-dependent aging factor is applied to the WEC failure rate. This factor is calibrated based on the conservative assumption that the failure rate will have doubled by the end of project life, representing the 'wear-out' phase of the system.
S4	Uncertain system reliability and maintainability	Due to technological advancements and market fluctuations affecting system components reliability, maintenance practices, and repair capabilities, system availability can exhibit inherent uncertainties. This scenario evaluates the effects of such uncertainties by varying system failure rates, repair times, and associated material costs by ±20%.

mooring failures by around 26%. Consequently, as shown in Fig. 21a, a total of 15.3 MAUD reduction is expected to be saved in project OPEX over the 20-year operational period. This outcome underscores the considerable economic benefits through enhanced wave-protection effect, providing strong motivation for further optimization of the system layout.

Additionally, beyond cost-saving advantages, reduced wave exposure is known to positively impact fish survivability and growth. Previous research by IMAS (Lacharite et al., 2021) suggests that lower wave height enhances survival rates and overall physiological stability of salmon, thereby improving their growth rate. As a result, an average increase in the salmon growth rate of 10% is implemented within this scenario. This adjustment is modelled by introducing a random scale factor to the original growth rate, which is sampled from a normal distribution ranging between 1.0 and 1.2, with a mean value of 1.1 and a standard deviation of 0.02. Similarly, a corresponding 5% reduction in salmon mortality rate is also incorporated into the SD model for this scenario. As the result, in each aquaculture farming cycle, approximately 8.5% increase in total fish production is accumulated by the end of the cycle (see Fig. 21b). This substantial increase in productivity is attributed to achieving better wave-protection effects.

S2: Fluctuating Aquaculture system power demand

In Scenario 2, the SD model quantified the robustness of WEC power supply under ±20% demand variability from the aquaculture farm. To simulate this scenario, an energy demand fluctuation factor, which follows a normal distribution ranging between 0.8 and 1.2, was implemented into the SD model. The model used this distribution for sampling energy demand fluctuations at each simulation time.

Fig. 22a shows the system's resultant net energy production, calculated as the WEC farm power production minus the aquaculture system's energy requirement. Negative values show the periods in which the WEC farm cannot fully meet the aquaculture power demand. Fig. 22b illustrates the cumulative duration of power shortages, which is only 15 h during the system life-cycle. Although this is deemed negligible, it demonstrates the capability of the developed SD model, which can be readily used to predict system power shortfall, particularly if other/increased usage is added to the system. It was noted that the shortage periods occurred when peaks in aquaculture demand coincided with decreased energy production due to WEC downtime.

Overall, the results suggest that the designed WEC farm reliably meets aquaculture energy needs even under notable demand fluctuations, underscoring its suitability for MPOP development to support offshore aquaculture farming.

S3: WEC system degradation

This scenario investigates the degradation of WEC devices on long-term system performance. In spite of regular maintenance, structural and mechanical components within the WEC devices will gradually age due to material degradation exacerbated by the corrosive ocean environment, marine loads, and operational wear. Consequently, a progressive increase in the failure rate of components is expected. To simulate this "wear-out" phase, the WEC failure rate is modelled as a time-dependent variable instead of a constant. In the SD model, a constant failure rate is adopted for the first five years (43,800 h) of operation. Beyond this point, the effect of WEC degradation is modelled as an increase in the failure rate. This effect is calibrated such that the effective failure rate doubles over the remaining 15 years.

Fig. 23a compares the temporal change in WEC farm availability between the degradation scenario and the baseline. Initially, the system experiences a transient phase of availability reduction lasting approximately 2000 operational hours, after which stabilizing at an availability level around 0.9 (shown in Fig. 23b). As the degradation occurs, the availability profile starts to decline. Even though repair activities continue, the increasing failure rate outpaces the unchanged repair rate. By the end of the 20-year life-cycle, the overall availability drops to 0.83.

The subsequent influence of this availability decline on the MPOP energy production is quantified in the SD model. The system energy production capacity decreases by approximately 5.6% compared to the non-degradation baseline. Despite this reduction, no energy shortages occurred throughout the MPOP lifespan, demonstrating robust system operational resilience against the WEC degradation.

S4: Effect of system reliability and maintainability

Technological development and market variability inherently influence system reliability and maintainability. This scenario evaluates the effects of uncertainties by using SD to assess both an optimistic (20% decreased failure rate, reduced CM time, and less material cost) and a pessimistic (20% increased failure rate and higher CM cost& time) occurrence of reliability performances.

Compared to the baseline, the pessimistic scenario elevates OPEX costs by 14.4%, as shown in Fig. 24. This increase primarily results from higher frequency of component failures, prolonged downtime, and subsequent energy production losses. Conversely, the optimistic scenario demonstrates 10.3% cost savings, underlining the economic benefits achievable through technological improvement and optimized maintenance practices.

3.10. Case study summary

This section demonstrates the practical applicability and robust capabilities of the developed SD framework through a detailed case study

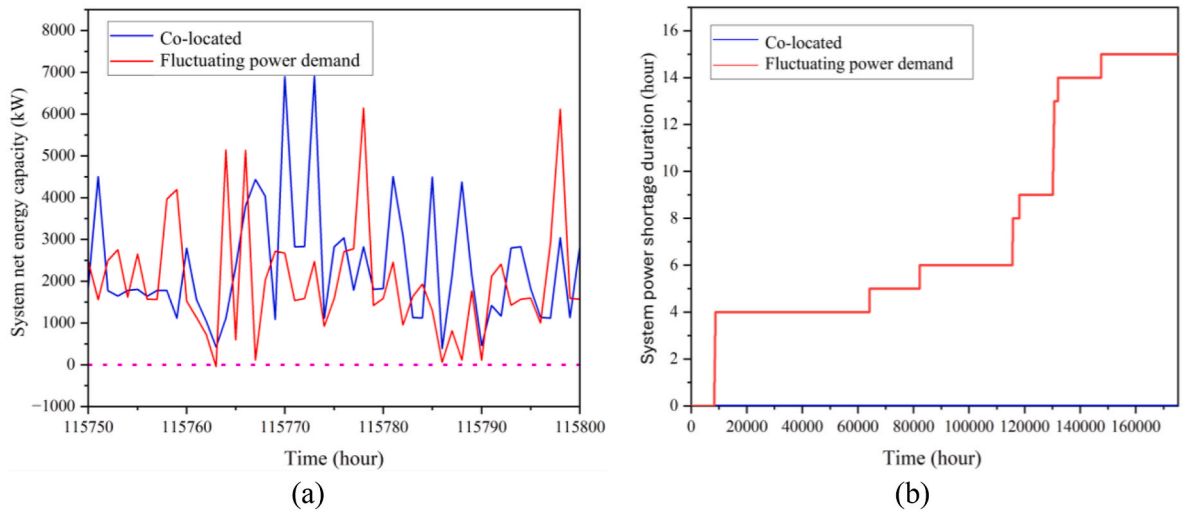

Fig. 22. Evaluated impacts of fluctuating aquaculture power demand on system operational performance, including a) net energy production, and b) accumulated power shortage duration.

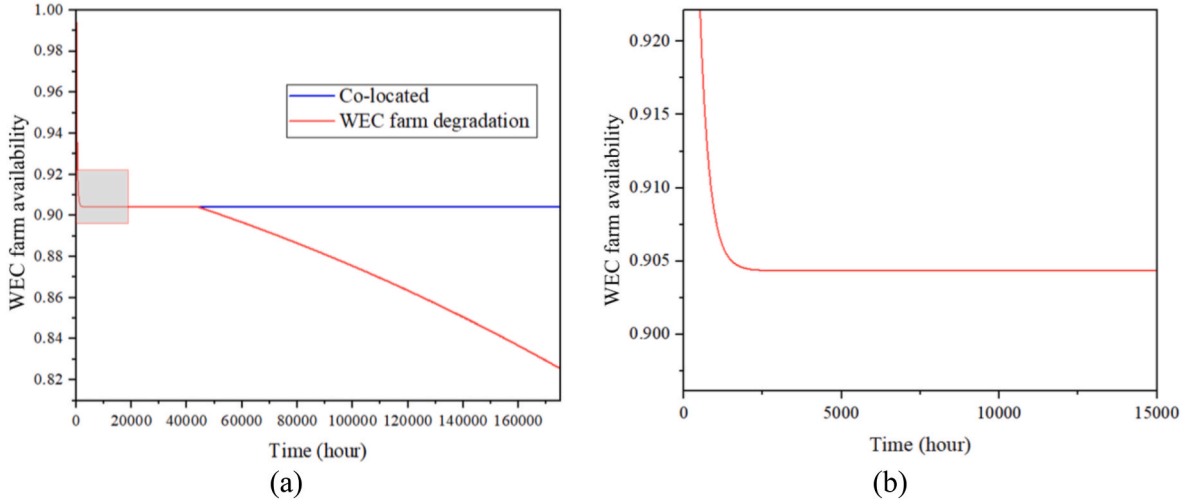

Fig. 23. Temporal change of WEC system availability, a) Comparison between the degradation scenario and baseline scenario and b) Close-up of the availability stable phase.

of a co-located WEC farm and aquaculture system. The case study directly addresses the real-world challenges associated with the offshore expansion of the Tasmanian salmon industry by quantitatively assessing the feasibility of the MPOP concept, specifically using a CETO 6 WEC farm to power and protect the downstream aquaculture facilities in harsh offshore environments.

By integrating hydrodynamic numerical simulations, probabilistic reliability modelling, and statistical analysis into the SD model, the framework successfully quantifies the system multi-domain performance. This model enables a detailed assessment of system energy and food production, as well as its life-cycle cost, while accounting for environmental and operational uncertainties.

Furthermore, the robustness of the model was validated through a comprehensive sensitivity analysis. By simulating various operational scenarios, including "maximum protection effects", "fluctuating aquaculture system energy demand", "WEC degradation", and "Uncertain system reliability and maintainability", the model demonstrates its capacity to reflect the impacts of critical operational uncertainties on system performance. The analysis shows that co-locating design can be a significant lever for the economic improvement, while the energy system design ensures resilience against long-term asset aging and demand fluctuations. These studies validate that the developed SD model can serve as a practical decision-making tool for complex offshore activities developments by accurately simulating their production capacity, economic feasibility and robustness against the operational uncertainties.

4. Conclusion

This study developed a hybrid quantitative framework to evaluate the operational performance, reliability, and economic feasibility of a co-located WEC and offshore aquaculture system. Addressing the gap in previous research that remains at conceptual or qualitative stages, this study identifies and quantifies the critical operational and environmental uncertainties of the MPOP and analyses their effects on system performance. By integrating numerical simulations, probabilistic modelling, and statistical analysis into a SD model, the model captures complex subsystems interactions and enables scenario-based evaluation of uncertain parameters in offshore operations.

The results demonstrate significant synergy benefits from co-locating offshore aquaculture systems with a WEC farm. Simulated shadowing effects of the upstream WEC farm effectively reduced downstream wave heights by approximately 8%–23%, which in turn lowered aquaculture

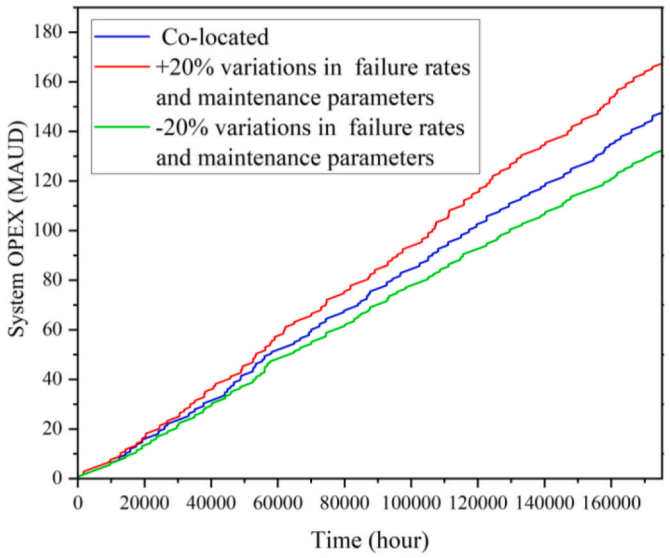

Fig. 24. System accumulated OPEX comparison under uncertain reliability and maintainability scenarios.

cages anchor-line tensions by about 2%–18%. These load reductions improved operational reliability by reducing critical structural failures and associated maintenance. Economically, the co-located configuration outperformed stand-alone offshore energy and aquaculture operations, with life-cycle cost savings of approximately 30.7% due to reduced diesel use, more efficient PM vessel utilisation, and lower CM expenditure. Specifically, under maximum shadowing effect, additional operational cost savings of approximately 15.3 MAUD and an 8.5% increase in aquaculture productivity per farming cycle can be achieved. From an energy perspective, the WEC system demonstrates robust and reliable power production capabilities for aquaculture operations. Scenario analyses indicate that the WEC farm can consistently supply surplus energy, even when facing uncertain aquaculture energy demands and facility performance degradation.

Overall, this study contributes to advancing the understanding of life-cycle operation of co-located offshore renewable energy and aquaculture systems. The developed framework provides a comprehensive way to quantify the trade-offs among energy supply, aquaculture production, system reliability, and life-cycle cost under uncertain offshore conditions. In practice, the framework can be used in early system design and decision-making stage to identify the required WEC farm capacity and scale to support offshore aquaculture operations, evaluate system productivity, estimate operational cost, and test the robustness of candidate designs through scenario-based sensitivity analysis. Therefore, it provides quantitative evidence to inform the design of MPOPs and support stakeholders in making strategic decisions when evaluating co-located MPOP developments.

Future research could extend the application of the developed system dynamic approach to further optimise MPOP designs. The optimal configurations of the MPOP can be investigated. This can involve adjusting the WEC farm layout, the number of devices, and the spatial arrangements between WEC and aquaculture facilities to maximise synergy effects and system performance. In addition, future work could extend the developed framework to multiple sites with different offshore environments to support location selection for MPOP operation. The framework also has the potential to be expanded to simulate more co-locating opportunities. Besides the wave energy and aquaculture, it can be used to evaluate other ocean renewable energy sectors and integrate a wider range of offshore activities. This would improve the off-grid surplus energy usage and broaden the feasibility and application potential of the MPOP system across various offshore environments.

CRediT authorship contribution statement

Minghan Bao: Writing – original draft, Visualization, Validation, Software, Methodology, Formal analysis, Conceptualization. **Ehsan Arzaghi:** Writing – review & editing, Supervision, Resources, Project administration, Conceptualization. **Rouzbeh Abbassi:** Writing – review & editing, Supervision, Resources, Project administration, Funding acquisition, Conceptualization.

Declaration of competing interest

The authors declare that they have no known competing financial interests or personal relationships that could have appeared to influence the work reported in this paper.

Acknowledgement

The authors acknowledge the financial support of the Blue Economy Cooperative Research Centre, established and supported under the Australian Government's Cooperative Research Centres Program, grant number CRC-20180101.

References

National map. https://nationalmap.gov.au/.
Abhinav, K., et al., 2020. Offshore multi-purpose platforms for a blue growth: a technological, environmental and socio-economic review. Sci. Total Environ. 734, 138256.
ABS, 2012. Guidance notes on the application of synthetic ropes for offshore mooring. American Bureau of Shipping (ABS) Drive Spring, TX.
Agency, I.E., 2025. Global Energy Review 2025. International Energy Agency Paris, France.
Agyekum, E.B., Khan, T., Ampah, J.D., Giri, N.C., Mbasso, W.F., Kamel, S., 2024. Review of the marine energy environment-a combination of traditional, bibliometric and PESTEL analysis. Heliyon 10 (6), e27771.
Aryai, V., et al., 2021. Reliability of multi-purpose offshore-facilities: present status and future direction in Australia. Process Saf. Environ. Prot. 148, 437–461.
Bao, M., et al., 2024a. Site selection for offshore renewable energy platforms: a multi-criteria decision-making approach. Renew. Energy 120768.
Bao, M., et al., 2024b. Site selection for offshore renewable energy platforms: a multi-criteria decision-making approach. Renew. Energy 229, 120768.
BOM. "Sea Temperatures and Currents." Australian government bureau of meteorology. https://www.bom.gov.au/oceanography/forecasts/(accessed.
Brodtkorb, P.A., Johannesson, P., Lindgren, G., Rychlik, I., Rydén, J., Sjö, E., 2000. WAFO-a Matlab toolbox for analysis of random waves and loads. In: ISOPE International Ocean and Polar Engineering Conference. ISOPE. ISOPE-I-00-264.
Bujas, T., Koričan, M., Vukić, M., Soldo, V., Vladimir, N., Fan, A., 2022. Review of energy consumption by the fish farming and processing industry in Croatia and the potential for zero-emissions aquaculture. Energies 15 (21), 8197.
Carnegie. "CETO technology." https://www.carnegiece.com/ceto-technology/(accessed.
Cifuentes Salazar, C.A., 2016. Dynamic Analysis of Cage Systems Under Waves and Current for Offshore Aquaculture.
Crawford, C., Macleod, C.K., Mitchell, I., 2002. Evaluation of Techniques for Environmental Monitoring of Salmon Farms in Tasmania.
Electricity, G., 2020. Projected Costs of Generating Electricity, ed: B.
EuropeanUnion, 2014. Directive 2014/89/EU of the European parliament and of the council of 23 July 2014 establishing a framework for maritime spatial planning [Online]. Available: http://data.europa.eu/eli/dir/2014/89/oj.
Faltinsen, O.M., Shen, Y., 2018. Wave and current effects on floating fish farms: keynote contribution for the international workshop on wave loads and motions of ships and offshore structures, Harbin, China, 5-7 November, 2017. J. Mar. Sci. Appl. 17 (3), 284–296.
FAO, 2024. The State of World Fisheries and Aquaculture 2024 Blue Transformation in Action.
Fløysand, A., Lindfors, E.T., Jakobsen, S.-E., Coenen, L., 2020. Place-based directionality of innovation: tasmanian salmon farming and responsible innovation. Sustainability 13 (1), 62.
Freeman, M., Garavelli, L., Wilson, E., Hemer, M., Abundo, M., Travis, L.E., 2022. Offshore aquaculture: a market for ocean renewable energy. Report for Ocean Energy Systems (OES).
Garavelli, L., Freeman, M.C., Tugade, L.G., Greene, D., McNally, J., 2022. A feasibility assessment for co-locating and powering offshore aquaculture with wave energy in the United States. Ocean Coast Manag. 225, 106242.
Geary, W.L., et al., 2020. A guide to ecosystem models and their environmental applications. Nat. Ecol. Evol. 4 (11), 1459–1471.
Gielen, D., et al., 2019. Global Energy Transformation: a Roadmap to 2050.
Göteman, M., Mathew, J., Engström, J., Castellucci, V., Giassi, M., Waters, R., 2018. Wave energy farm performance and availability as functions of weather windows. In: Advances in Renewable Energies Offshore: Proceedings of the 3rd International

Conference on Renewable Energies Offshore (RENEW 2018), October 8-10, 2018. CRC Press, Lisbon, Portugal, p. 73.
Griffin, R., Buck, B., Krause, G., 2015. Private incentives for the emergence of co-production of offshore wind energy and mussel aquaculture. Aquaculture 436, 80–89.
Guo, Q., Xu, Z., 2011. Simulation of deep-water waves based on JONSWAP spectrum and realization by MATLAB. In: 2011 19th International Conference on Geoinformatics. IEEE, pp. 1–4.
Hemer, M.A., et al., 2017. A revised assessment of Australia's national wave energy resource. Renew. Energy 114, 85–107.
Hemer, M., Franklin, E., Hayward, J., Shoushtari, M.A., 2020. Energy Demand Analysis of Offshore Aquaculture. A Report for the Blue Economy Co-operative Research Centre.
IEA, 2021. Net Zero by 2050. International Energy Agency (IEA), Paris [Online]. Available: https://www.iea.org/reports/net-zero-by-2050.
Kamidelivand, M., et al., 2024. Failure consequence cost analysis of wave energy converters—component failures, site impacts, and maintenance interval scenarios. J. Mar. Sci. Eng. 12 (8), 1251.
Kumar, S., Arzaghi, E., Baalisampang, T., Abaei, M.M., Garaniya, V., Abbassi, R., 2024. A risk-based multi-criteria decision-making framework for offshore green hydrogen system developments: pathways for utilizing existing and new infrastructure. Sustain. Prod. Consum. 46, 655–678.
Lacharite, M., Ross, D., Adams, V., Bush, F., Byers, R., 2021. Statewide Finfish Aquaculture Spatial Planning Exercise: Investigating Growth Opportunities for Finfish Aquaculture in Tasmanian Coastal Waters.
Lavelle, J., Kofoed, J.P., 2013. Representative spectra of the wave resource from real sea wave measurements. In: European Wave and Tidal Energy Conference. Technical Committee of the European Wave and Tidal Energy Conference.
Li, L., Bruset, M., Ong, M.C., Wu, X., 2020. Numerical analysis of a floating fish cage with feeding systems. In: International Conference on Offshore Mechanics and Arctic Engineering, vol. 84362. American Society of Mechanical Engineers p. V005T05A001.
Liu, J., et al., 2023. A high-resolution wave energy assessment of south-east Australia based on a 40-year hindcast. Renew. Energy 118943.
López-Ruiz, A., Bergillos, R.J., Raffo-Caballero, J.M., Ortega-Sánchez, M., 2018. Towards an optimum design of wave energy converter arrays through an integrated approach of life cycle performance and operational capacity. Appl. Energy 209, 20–32.
Ma, M., Ong, M.C., Strauss, D., Zhang, H., 2025. Assessment of long-term wave conditions and the spatial variability for fish farming zones. Ocean Eng. 341, 122787.
Meng, H., Hayashida, H., Norazmi-Lokman, N.H., Strutton, P.G., 2022. Benefits and detrimental effects of ocean warming for Tasmanian salmon aquaculture. Cont. Shelf Res. 246, 104829.
Menicou, M., Vassiliou, V., 2010. Prospective energy needs in Mediterranean offshore aquaculture: renewable and sustainable energy solutions. Renew. Sustain. Energy Rev. 14 (9), 3084–3091.
MOWI, 2020. Salmon Farming Industry Handbook 2020. Mowi ASA [Online]. Available: https://mowi.com/wp-content/uploads/2020/06/Mowi-Salmon-Farming-Industry-Handbook-2020.pdf.
Nasyrlayev, N., Dyson, A.P., Kefayati, G., Tolooiyan, A., 2023. Modelling the response of offshore aquaculture fish pens to environmental loads in high-energy regions. Appl. Ocean Res. 135, 103541.
Niosi, F., et al., 2023. Experimental validation of Orcaflex-based numerical models for the PEWEC device. Ocean Eng. 281, 114963.
Onea, F., Rusu, E., 2019. The expected shoreline effect of a marine energy farm operating close to sardinia island. Water 11 (11), 2303.
Orcaflex. Orcaflex help. https://www.orcina.com/webhelp/OrcaFlex/.
Orcina, L., 2016. OrcaFlex User Manual Version 11.0 B. Orcina Ulverston, UK.
Orszaghova, J., Wolgamot, H., Draper, S., Rafiee, A., 2018. Motion instabilities in tethered buoy WECs. In: 4th Asian Wave and Tidal Energy Conference 2018.
Orszaghova, J., Wolgamot, H., Draper, S., Taylor, P.H., Rafiee, A., 2020. Onset and limiting amplitude of yaw instability of a submerged three-tethered buoy. Proceedings of the Royal Society A 476 (2235), 20190762.
Paduano, B., et al., 2020. Experimental validation and comparison of numerical models for the mooring system of a floating wave energy converter. J. Mar. Sci. Eng. 8 (8), 565.
Prendergast, J., Li, M., Sheng, W., 2018. A study on the effects of wave spectra on wave energy conversions. IEEE J. Ocean. Eng. 45 (1), 271–283.
Ranganathan, J., Waite, R., Searchinger, T., Hanson, C., 2018. How to sustainably feed 10 billion people by 2050, in 21 charts. World Resources Institute 5.
Rhinefrank, K., 2016. StingRAY Failure Mode, Effects and Criticality Analysis: WEC Risk Registers[data set].
Rijnsdorp, D.P., Hansen, J.E., Lowe, R.J., 2020. Understanding coastal impacts by nearshore wave farms using a phase-resolving wave model. Renew. Energy 150, 637–648.
Rosenberg, B.J., et al., 2019. Development of WEC Design Loads: a Comparison of Numerical and Experimental Approaches. National Renewable Energy Lab.(NREL), Golden, CO (United States).
Ruehl, K.M., Roberts, J.D., Posner, A., Porter, A., 2013. Development of SNL-SWAN a Validated Wave Energy Converter Array Modeling Tool. Sandia National Lab.(SNL-NM), Albuquerque, NM (United States).
Sergiienko, N.Y., Cocho, M., Cazzolato, B.S., Pichard, A., 2021. Effect of a model predictive control on the design of a power take-off system for wave energy converters. Appl. Ocean Res. 115, 102836.
Shen, Y., Greco, M., Faltinsen, O.M., Nygaard, I., 2018. Numerical and experimental investigations on mooring loads of a marine fish farm in waves and current. J. Fluid Struct. 79, 115–136.
Silva, D., Rusu, E., Guedes Soares, C., 2018. The effect of a wave energy farm protecting an aquaculture installation. Energies 11 (8), 2109.
Stead, S.M., Laird, L., 2002. The Handbook of Salmon Farming. Springer Science & Business Media.
Stokes, C., Conley, D.C., 2018. Modelling offshore wave farms for coastal process impact assessment: waves, beach morphology, and water users. Energies 11 (10), 2517.
Syse, H.L., 2016. Investigating off-grid Energy Solutions for the Salmon Farming Industry. University of Strathclyde, Glasgow, UK.
Tang, H.-J., Yeh, P.-H., Huang, C.-C., Yang, R.-Y., 2020. Numerical study of the mooring system failure of aquaculture net cages under irregular waves and current. Ocean Eng. 216, 108110.
Têtu, A., Fernandez, C., 2020. Deliverable D8. 1—Cost database. LiftWEC-Development of a new class of wave energy converter based on hydrodynamic lift forces, Tech. Rep.
Turschwell, M., et al., 2022. A review of support tools to assess multi-sector interactions in the emerging offshore blue economy. Environ. Sci. Pol. 133, 203–214.
Verao Fernandez, G., Stratigaki, V., Quartier, N., Troch, P., 2021. Influence of power take-off modelling on the far-field effects of wave energy converter farms. Water 13 (4), 429.
WorldBank, 2017. The Potential of the Blue Economy. World Bank Group & United Nations Department of Economic and Social Affairs [Online]. Available: https://openknowledge.worldbank.org/bitstream/handle/10986/26843/115545.pdf?sequence=1&isAllowed=y.